

March 24 – to appear in ApJS

Rotational modulation of X-ray emission in Orion Nebula young stars

E. Flaccomio¹, G. Micela¹, S. Sciortino¹, E. D. Feigelson², W. Herbst³, F. Favata⁴, F.R. Harnden Jr.^{5,6} and S. D. Vrtilek⁵

ettoref@astropa.unipa.it

ABSTRACT

We investigate the spatial distribution of X-ray emitting plasma in a sample of young Orion Nebula Cluster stars by modulation of their X-ray light-curves due to stellar rotation. The study, part of the *Chandra Orion Ultradeep Project* (COUP), is made possible by the exceptional length of the observation: 10 days of ACIS integration during a time span of 13 days, yielding a total of 1616 detected sources in the 17×17 arcmin field of view. We here focus on a subsample of 233 X-ray-bright stars with known rotational periods. We search for X-ray modulation using the Lomb Normalized Periodogram method.

X-ray modulation related to the rotation period is detected in at least 23 stars with periods between 2 and 12 days and relative amplitudes ranging from 20% to 70%. In 16 cases, the X-ray modulation period is similar to the stellar rotation period while in seven cases it is about half that value, possibly due to the presence of X-ray emitting structures at opposite stellar longitudes. These results constitute the largest sample of low mass stars in which

¹INAF-Osservatorio Astronomico di Palermo Giuseppe S. Vaiana, Piazza del Parlamento 1, 90134 Palermo, Italy

²Department of Astronomy and Astrophysics, 525 Davey Laboratory, Pennsylvania State University, University Park, PA 16802, U.S.A

³Department of Astronomy, Wesleyan University, Middletown, CT 06459, U.S.A

⁴Astrophysics Division, Research and Science Support Dept. of ESA, Postbus 299, 2200 AG Noordwijk, The Netherlands

⁵Smithsonian Astrophysical Observatory, 60 Garden St., Cambridge, MA 02138, U.S.A

⁶Universe Division, Science Mission Directorate NASA Headquarters

X-ray rotational modulation has been observed. The detection of rotational modulation indicates that the X-ray emitting regions are distributed inhomogeneously in longitude and do not extend to distances significantly larger than the stellar radius. Modulation is observed in stars with saturated activity levels ($L_X/L_{bol} \sim 10^{-3}$) showing that saturation is not due to the filling of the stellar surface with X-ray emitting regions.

1. Introduction

Pre-main Sequence (PMS) stars have high levels of X-ray activity with non-flaring X-ray luminosities up to 10^{31} erg s $^{-1}$ (Preibisch et al. 2005). As in the case of older cluster and field stars, X-ray activity in the PMS phase has often been attributed to a “scaled up” solar-like corona formed by active regions but more densely packed on the stellar surface and/or having higher plasma densities than on the Sun. For most non-accreting PMS stars (Weak-line T-Tauri Stars, WTTS), the fraction of energy emitted in the X-ray band with respect to the total stellar output, L_X/L_{bol} , is close to the saturation level, 10^{-3} , seen on rapidly rotating main sequence (MS) stars (Flaccomio et al. 2003b; Preibisch et al. 2005; Pizzolato et al. 2003). This suggests a common physical mechanism for the emission of X-rays or, at least, for its saturation in PMS and MS stars.

However, the solar analogy, while providing a simple picture of activity in PMS stars, may not be fully valid. Saturated PMS stars have $L_X/L_{bol} \sim 1000$ times greater than the Sun at its maximum, when the solar surface is $\sim 50\%$ covered with active regions and $\sim 1\%$ covered with active regions cores (Drake et al. 2000; Orlando et al. 2001). Plasma temperatures in saturated stars are much higher than on the Sun and, in the few cases where surface distributions can be determined, their active regions are concentrated at higher latitudes (e.g. Favata & Schmitt 1999, Jardine et al. 2002). The nature of the saturation phenomenon is not understood. It might be due to filling of the stellar surface with active regions, saturation of the magnetic reconnection process that heats the plasma, centrifugal limits on the coronal extent, concentration of magnetic fields towards the poles, or saturation of the internal dynamo generating the magnetic field that confines the plasma (Güdel 2004).

Even more puzzling than WTTS are PMS stars that are still undergoing mass accretion (Classical T-Tauri Stars, CTTS). CTTS, with their circumstellar disks and magnetically funneled matter inflows and outflows host in general several different physical phenomena. With respect to X-ray activity, the bulk of the observational evidence points toward phenomena similar to those occurring on WTTS. However, CTTS have significantly lower and unsaturated values of L_X and L_X/L_{bol} (Damiani & Micela 1995; Flaccomio et al. 2003a,b; Preibisch et al. 2005). Similar to saturated WTTS, their X-ray activity does not correlate

with stellar rotation, as seen in unsaturated MS stars and naturally interpreted in terms of a rotationally regulated $\alpha - \Omega$ dynamo. A further complication is that the high-resolution X-ray spectra of two observed CTTS, TW Hya (Kastner et al. 2002; Stelzer & Schmitt 2004) and BP Tau (Schmitt et al. 2005), indicate that a fraction of the soft X-ray luminosity may be produced in accretion shocks rather than coronal magnetic reconnection events.

In contrast to emission close to the stellar surface, some of the strongest flares seen in PMS stars are most easily explained by magnetic loops connecting the stellar surface with a circumstellar disk (Favata et al. 2005). Such loops arise naturally in models of magnetically driven accretion that seem to best explain the shapes of optical emission lines (Shu et al. 1994; Muzerolle et al. 2001). Magnetic reconnection in these loops might be the source of powerful and long-lasting X-ray flares (e.g. Shu et al. 1997; Montmerle et al. 2000). The influence of circumstellar disks and/or accretion on the emission of X-rays is not altogether unexpected given that the stellar magnetic field responsible for the confinement of X-ray emitting plasma is likely affected by the circumstellar environment.

Observations of rotationally induced modulation of X-ray emission from low mass stars can potentially yield valuable information on the extent and spatial distribution of the magnetic structures in active stars. Such observations are to date very scarce. X-ray rotational modulations have been seen in VXR 45, a fast rotating ($P_{rot} = 0.22$ d) G9 ZAMS star (Marino et al. 2003), AB Dor (Hussain et al. 2005), a K0 ZAMS star with $P_{rot} = 0.5$ d, and possibly EK Dra ($P_{rot} = 2.7$ d) (Guedel et al. 1995). To the authors' knowledge, X-ray rotational modulation has not been to date reported for any PMS star. Because of the typical duration of X-ray observations, ~ 1 day, it is indeed difficult to detect rotational modulation in the majority of stars which have much longer periods.

The *Chandra* Orion Ultradeep Project (COUP) has detected over 1616 sources in an 850 ks exposure spanning 13.2 d of the rich young Orion Nebula Cluster (ONC Getman et al. 2005), well in the range of optically determined periods of PMS stars (Herbst et al. 2002). With COUP, we thus have the unique opportunity to study rotational modulation of X-ray emission on a large sample of PMS stars. We focus here on COUP sources whose rotation period is known from optical studies. Results from the analysis method discussed below are also presented for specific COUP sources by Stelzer et al. (2005) and Grosso et al. (2005).

The paper starts with a definition of the catalog of COUP sources with known rotation periods (§2). Section 3 describes the X-ray light curves and the analysis method used to estimate X-ray modulation periods and their reliability. Results of the period search are presented in §4, followed by discussion of implications for the physical origin of X-ray activity in PMS stars (§5). Finally in §6 we summarize our results.

2. Catalogs of optical periods

Our primary goal is to establish whether rotational modulation of X-ray emission is observed in COUP sources. Our initial sample comprises 295 COUP sources for which we could find in the literature a rotational period (P_{opt}) determined from the periodic modulation of optical or near-infrared light curves.

We started with the list of 201 optical periods measured by Herbst et al. (2002) and reported by Getman et al. (2005) for COUP sources. Two of these COUP sources, 150 and 1328, are identified with close pairs: COUP 150 with sources 010-411 and 011-410 in Lucas & Roche (2000) and with sources 201 and 10342 in Herbst et al. (2002)¹, of which only 201 has a rotation period. COUP 1328 is associated with both 776a (with measured rotation period) and 776b in Hillenbrand (1997, hereafter H97). In both cases, following Getman et al. (2005), we associated the X-ray source with the rotation period measured by Herbst et al. (2002) for one of the components. Our search for modulation in the X-ray light curves yields periods that appear related to these optically determined periods, thus confirming the association. We exclude the rotation period listed by Getman et al. (2005) for COUP 460, associated with source 347 in the catalog of Jones & Walker (1988, hereafter JW), for which we could not find an optical period in the literature. Furthermore, we have updated the optical periods for COUP 1432 (JW 843, $P=5.38\text{d}$), 1443 (JW 852, $P=1.32\text{d}$) and 1487 (JW 883, $P=5.70\text{d}$), based on unpublished improved determinations by W. Herbst.

We then added periods from recent literature: 51 from Herbst et al. (2000); 15 from Stassun et al. (1999); 23 from the list of Carpenter et al. (2001) (selecting only periods with $\text{FAP} < 1\%$); 3 from Herbst et al. (2002) missed by Getman et al. (2005) (COUP 3 = JW 25, $P=2.28\text{d}$; COUP 68 = JW 130, $P=1.2\text{d}$; COUP 252 = JW 275a, $P = 0.95\text{d}$); and 3 unpublished by W. Herbst (COUP 328 = JW 330, $P=4.08\text{d}$; COUP 1350 = JW 795, $P=2.80\text{d}$; COUP 1154 = JW 684, $P=3.35\text{d}$).

Table 1 lists the 295 COUP sources that are thus assigned a rotational period. In cases when more than one optical period was retrieved from the literature, we list other values if differing by more than 10% from the adopted one.

¹Entries for source 201 and 10342 in Herbst et al. (2002) are very similar and they might actually refer to the same object, but only 201 has a rotation period. Source 010-411 and 011-410 in Lucas & Roche (2000) are $1.1''$ apart (seeing $\sim 0.6''$) and have similar magnitudes and colors. The H magnitudes add up to the 2MASS value of 10.6, but the J magnitudes add up to 10.05 while 2MASS gives 11.48.

3. X-ray light curves and analysis method

Adopting the source photon extraction of the ACIS X-ray data presented in Getman et al. (2005), we bin arrival times and compute the count rate in each bin taking into account gaps in the observation. We then subtract the mean background count rate² as determined from a source-free region close to each source (Getman et al. 2005). The period analysis described below was originally performed with bin lengths of 10000, 5000, and 2000 seconds. Results obtained in the three cases were very similar, both regarding the modulation periods found and their statistical significances, though slightly better significances were obtained with shorter bin lengths, probably as a result of an improved ability to account for non-rotationally induced variability (e.g. flares). In the following, we therefore refer exclusively to the analysis performed using 2000 seconds bins.

Our goal is to detect rotational modulation in the X-ray light curves of COUP sources. We have initially considered two period analysis methods: the Lomb Normalized Periodogram (LNP) method (Scargle 1982) and the string length method (SLM) with length defined as in Lafler & Kinman (1965), but soon realized that the former gave better results. The LNP is the traditional Schuster (1898) periodogram of Fourier analysis adjusted for gaps in the data: a function is computed from the data for a range of test frequencies and the frequency that maximizes this function is considered as the most likely frequency in the data.

In order to estimate the range of applicability of the LNP analysis to our data we first performed a series of simple simulations by generating purely periodic light curves in 2000 s bins with the observed window function. Three lightcurve shapes were considered: a sinusoid ($M[1 + A \sin \omega t]$), a three level ($M[1 - A], M, M[1 + A]$) step function, and a two level ($M[1 - A], M[1 + A]$) step function. Simulated periods ranged from 0.5 to 30 days and relative amplitudes (A) from 10% to 90%. Noise was assumed Poissonian, appropriate for total source counts ranging from 100 to 10^5 . One hundred replicates were run for each set of input parameters. Figure 1 shows the results for the cases of sinusoidal light curves and $A = 30\%$ and $A = 90\%$. The plots show the median and the 1σ dispersion of the ratio between the period corresponding to the main LNP peak (P_{out}) and the input period P_{in} as a function of input period and simulated source counts. Note that, at this stage, we are not yet estimating significances for the peaks in the periodograms as in the more sophisticated simulations discussed in Sect. 4.2. The simulations here indicate that a certain fraction of the P_{out} will be unrelated to P_{in} when the statistics and/or the amplitudes are too low. In

²For all sources the background rate is statistically indistinguishable from being constant within the observation.

the $A = 30\%$ case, for example, the curves referring to the 100 count lightcurves lie outside the plot vertical scale. For high count rates, the median P_{out}/P_{in} does not diverge by more than 0.03 dex for $P_{in} < 13$ days, the length of the observation (including gaps in the data stream). For simulations with 100 (1000) counts, the minimum amplitude that still yields $P_{in}/P_{out} \sim 1$ for $P_{in} < 13$ d is $A \sim 60\%$ (20%). Similar results are obtained if the shape of the simulated modulation is changed from a sinusoid to a 2 or 3 level step function.

Given these results, in the analysis of real data we therefore decided to limit our search to X-ray periods P_X shorter than 13 days. The lower limit to the accessible P_X is set by timescales of the non-rotational variability present in our data, notably flares. Because of variability unrelated to rotation, the simulation discussed above represent a best case scenario and can only indicate a lower limit to the typical uncertainties in the determination of periods. In Sect. 4.2, after presenting the results of the LNP analysis of COUP sources, we introduce more realistic simulations of light curves that include flares.

3.1. Calculation of FAPs and filtering of light curves

The most difficult part of the periodogram analysis in the non-ideal case is establishing the significance of the peaks found in the LNP or, more specifically, the false alarm probabilities (FAPs). Stochastic noise and intrinsic variability, unrelated to rotational modulation can produce spurious features in the LNP that can easily be mistaken for real modulation. A simple example, which recurs frequently in our data, is that of repeated flares. Two bright flares occurring on the same source within our observation with a temporal separation ΔT will produce a spurious peak in the periodogram at frequency $1/\Delta T$. It is therefore paramount to either take into account the non-rotationally induced variability in the calculation of the FAPs and/or to filter out identifiable features from the light curves prior to the calculation of the LNP.

In the presence of uncorrelated noise, FAPs can be computed from the actual light curve through a permutation resampling technique. A large number of artificial light curves are computed by replacing actual count-rates with values randomly chosen from the same light curve. The LNP analysis is then performed on each of these realizations and, for each frequency, the distribution of power values is recorded. Once the maximum from the real periodogram is found, its value can be compared to the distribution obtained, at the same frequency, from the randomized light curves in order to establish the probability that values as high as the observed one are due to random fluctuations; this is the FAP.

Performing this calculation for our X-ray light curves always results in vanishingly small

FAPs, indicating that LNPs of COUP sources present peaks that cannot be explained by purely stochastic noise. This arises because flares with a variety of characteristics are ubiquitous (Wolk et al. 2005; Favata et al. 2005), as well as less well-understood temporal phenomena. We therefore seek to compute FAPs by randomizing any periodic component of the light curves but preserving these other correlated features. We define blocks of adjacent temporal bins with total length τ_{corr} , and randomize the position of these blocks. Our τ_{corr} should be longer than flare timescales and shorter than rotational periods, but these two conditions cannot always be simultaneously achieved. We choose $\tau_{corr} = 8$ hours and consequently limit our search of peaks in the periodograms to periods longer than 1 day. We caution that the choice of $\tau_{corr} = 8$ hours is somewhat arbitrary and a number of longer flares are observed (Favata et al. 2005). For this reason the FAPs that we derive are not formally accurate, but we are confident they are good indicators of the relative significance of the peaks in the periodograms.

An essential element of our analysis is to perform periodogram analysis on both the original lightcurves and those where large flares are removed. We filter the lightcurves using two trimming levels established to qualitatively remove obvious flares: 1) a light trimming (“L”) of bins with count rates higher than 1.5 times the 13% upper quantile of the count rate distribution; and 2) a heavy trimming (“H”) of bins with count rates higher than 1.5 times the 25% quantile. We also tried filtering out time interval that are identified as belonging to flares using Maximum Likelihood Blocks as described in Wolk et al. (2005), but, except for a few sources, results were not in general better than with the simpler count rate trimming procedures. The original lightcurves will be referred to as “N” (no filter). Given the large variety of behaviors observed in our light curves, we have not been able to identify a single best filtering method for all cases. Moreover, our filtering may not always improve our ability to find real modulation periods and to reject spurious results due, for instance, to the alignment of untrimmed flare decay tails.

Given the above considerations on the possible pitfalls involved in the search for true modulation periods in the complex X-ray lightcurves of COUP sources, we adopt the following graduated levels of confidence in a possible rotational period detection: periodogram peaks are considered most significant when $\text{FAP} < 0.1\%^3$ in all three (“N”, “L”, and “H”) lightcurves. Less confidence is given to sources where $\text{FAP} < 0.1\%$ in any of the three lightcurves. When more than one filtering strategy exhibit a signal, we adopt the period with the lowest FAP⁴.

³FAPs were computed with the bootstrapping procedure described in this section using 100,000 iterations, sufficient to define the 0.1% level

⁴In 7 cases more than one LNP peak has $\text{FAP} = 0.0\%$ within the precision of the determination. In these

4. Results

Table 1 lists optical and X-ray data for the 295 COUP sources with known optical rotation periods. The period values are described in §2 and the remaining columns are obtained from tables in Getman et al. (2005). We performed the LNP period analysis for 233 of these sources; twenty-one sources with <100 X-ray photons and 41 sources with optical rotation period $P < 2$ d were omitted from analysis. This is to exclude stars for which period detection would likely be hampered by low photon statistics and by the similarity between the flare and modulation timescales. For the 233 analyzed sources, the last column indicates whether a $\text{FAP} < 0.1\%$ peak is seen in the periodogram of the ‘N’, ‘L’ and ‘H’ lightcurves. One hundred and nine sources are detected as periodic in at least one dataset (we call this the “ $N + L + H$ ” sample), 48 sources of these are detected as periodic using unfiltered (the N sample) lightcurves, and 34 of these are the highest confidence periodic signals showing a significant peak in all three datasets (the “ $N \cdot L \cdot H$ ” sample). Detailed results of the periodogram analysis for the $N \cdot L \cdot H$ sample are given in Table 2. For each source, we provide modulation periods and FAPs for each of the three X-ray light curves. The lowest FAP value (highest significance period) was obtained from the unfiltered light curves in 4 sources, lightly filtered lightcurves in 15 sources, and heavily filtered lightcurves in 15 sources (column 12 of Table 2).

The 13th column in Table 2 reports an estimate for the relative amplitude of the modulation from the folded X-ray lightcurve derived from the lightcurve giving the lowest FAP. In order to reduce random fluctuations when estimating amplitudes, we rebin the phased lightcurve to give 8 bins per modulation cycle if the lightcurve has less than 8000 counts and an average of 1000 counts per bin for brighter sources. The relative amplitude is then defined as the difference between the minimum and maximum count rates divided by the sum of the same quantities. Resulting values are uniformly distributed between $\sim 20\%$ and $\sim 70\%$.

Figures 2-4 show results in four panels for six illustrative COUP sources, three of which belong to the “ $N \cdot L \cdot H$ ” sample. We show: the original unfiltered lightcurves, the LNP periodograms for the best filtering strategy (i.e. lowest FAP), and lightcurves folded with both the best X-ray period and the previously known optical period. Similar figures for the 34 $N \cdot L \cdot H$ sources in table 2 are presented in the electronic edition of the Journal (Figure 15).

cases we choose the highest LNP peak above the $\text{FAP}=0.1\%$ threshold.

4.1. Statistical comparison of P_{opt} vs. P_X

The three panels in Figure 5 compare the optical and X-ray periods for the three different subsamples discussed in the previous section: the 109 $N+L+H$ sources showing $\text{FAP} < 0.1\%$ in at least one filtered dataset; the 48 N sources showing periodicity in the unfiltered dataset; and the 34 $N \cdot L \cdot H$ sources. For the least reliable $N+L+H$ sample, no clear relationship between the X-ray and optical periods is seen, but for the high confidence $N \cdot L \cdot H$ sample, most of sources align close to the $P_X = P_{opt}$ and the $P_X = 0.5 \times P_{opt}$ loci.

To better define this effect, the distribution of ratios between X-ray and optically determined periods is investigated in Figure 6. Vertical lines indicate ratios of 1/4, 1/2, 1, 2 and 4. In all samples, we see a main peak corresponding to roughly equal X-ray and optical periods and a smaller but narrower peak corresponding to $P_X \sim 0.5 \times P_{opt}$. We interpret these plots as evidence that a substantial fraction of the X-ray periods are indeed related to the optically determined rotation periods, even though one is often a harmonic of the other. To strengthen this conclusion, we show in Figure 7 the distribution of P_X/P_{opt} for X-ray sources that did not pass our significance test, i.e. those for which $\text{FAP} > 0.1\%$ in all three ‘N’, ‘L’ and ‘H’ analyses (top), ‘N’ (center), and any of ‘N’, ‘L’ or ‘H’ (bottom). These distributions show little or no relation between optical and X-ray modulation, giving confidence that the $\text{FAP} > 0.1\%$ criterium is indeed effective in preferentially selecting true X-ray modulation periods.

To facilitate discussion, we distinguish three types of COUP sources: class “1” when the X-ray and optical periods are nearly equal, $-0.05 < \log P_X/P_{opt} < 0.15$; class “ $\frac{1}{2}$ ” when the X-ray period is half of the optical period, $-0.3 < \log P_X/P_{opt} < -0.25$; and class “ \neq ” for all other stars. The light curves and periodograms in Figures 2-4 show two examples of each class. These classifications are listed in the last column of Table 2. Out of the 109 sources in sample $N+L+H$, 38, 14, and 57 belong to classes “1”, “ $\frac{1}{2}$ ” and “ \neq ” respectively. Out of the 34 sources in sample $N \cdot L \cdot H$, 16, 7 and 11 fall in the same classes⁵.

In addition to the expected finding of X-ray periods similar to the optical periods, we thus unexpectedly find X-ray periods half as long as established optical periods as well as a number of X-ray periods apparently unrelated to the stellar rotation. Moreover, within class “1” and “ $\frac{1}{2}$ ” sources, there is also a possible systematic shift such that P_X values are longer

⁵In some LNP periodograms of “ \neq ” sources, secondary peaks corresponding to $\sim P_{opt}$ or to $\sim 0.5P_{opt}$ are present. If we were to consider these secondary peaks as true modulation periods, seven “ \neq ” sources in the $N+L+H$ sample and one in the $N \cdot L \cdot H$ sample would be upgraded to class “1”.

than P_{opt} or $0.5 \times P_{opt}$ (Figure 5)⁶. It remains to be seen however whether these unexpected features in the P_X/P_{opt} ratio histogram are spurious effects due to the characteristic of the data and/or the analysis method we have applied.

4.2. Verification of the method through simulations

Due to the complexity of the COUP lightcurves and of our analysis procedures, in order to better understand our results, we have performed extensive Monte Carlo simulations of modulated and unmodulated lightcurves that try to reproduce the essential characteristics of our data. Construction of these simulated lightcurves, which include the complications of gaps in the *Chandra* exposure and flares in the COUP stars, are described in Appendix A. We then applied our full analysis method described in §3 to these simulated lightcurves. Here we summarize the main findings.

The dashed lines in Figures 6 and 7 indicate the expected outcome of our period analysis on simulated lightcurves that have no intrinsic periodicity, for reasonable choices of model input parameters. In each panel, different lines refer to different values of the parameters that determine the flare frequency distribution, the lightcurve statistics and the decay time of flares, all chosen so as to yield lightcurves that are reasonably similar to the observed ones (specifically, in particular, $\alpha = 2.50$, $NF = [500, 1000]$, $\tau_{fl} = [5, 8]\text{hr}$; see Appendix A). In all cases, these P_x/P_{opt} distributions do not show any sharp peak around 1.0 and 0.5 as we observe in the COUP data. We conclude that the presence of these peaks must be due to intrinsic source modulation. The fact that they occur at values of $P_X/P_{opt} \sim 1.0$ and 0.5, and not at any other values, is a further support that the X-ray modulations are real and related to stellar rotation.

In another important series of simulations we introduced periodic modulations into the simulated lightcurves. These simulation show that the observed spread in $\log P_X/P_{opt}$ among class “1” sources can be attributed to uncertainties in the analysis procedure. Moreover, all simulation series show that a fraction of sources show FAP<0.1% periods randomly distributed between $0.2 < P_X/P_{opt} < 5$. This can explain the observed sources with widely distributed P_X values in Figures 5 and 6. Our simulations do not however reproduce the subtle effect that P_X values tend to be slightly longer than P_{opt} in class “1” sources. Even more importantly they also fail to reproduce the second peak around $P_X/P_{opt} = 0.5$.

⁶We estimate the significance of the shifts, computing the mean $\log P_X/P_{opt}$ and its uncertainty in symmetrical intervals centered on 0 and $\log 0.5$. The shifts are most significant in the “N” sample: 3.2σ for the $P_X/P_{opt} \sim 1$ peak and 4.8σ for the $P_X/P_{opt} \sim 0.5$ peak

The fact that our simulations retrieve some of the fundamental characteristics of the real data after our complicated data analysis procedures lends strong support to the basic result that the class “1” and “ $\frac{1}{2}$ ” COUP sources are truly periodic with periods intrinsically related to the optical rotational periods.

4.3. Physical properties of modulated stars

We now return to the physical properties of the stars listed in Table 1 to investigate possible relationships to the stars showing rotational modulation. The “modulated” sub-sample showing rotational periodicities are the 23 class “1” and ” $\frac{1}{2}$ ” stars in the $N \cdot L \cdot H$ sample⁷. We compare these to the full sample of COUP sources searched for periodicities; i.e., the 233 “searched” sources with known P_{rot} , $P_{rot} > 2$ d and with more than 100 detected counts. Moreover, in order to understand possible biases in this latter sample, we will compare the “searched” sample to the “global” sample of COUP sources with more than 100 COUP counts.

Figure 8 shows the Hertzsprung-Russell diagram for these three samples. A comparison of the mass and age distributions of the “searched” and “global” samples indicate that the former is preferentially deficient in very low mass stars and also in the youngest population. This may be understood as a selection effect: very-low-mass stars are both less likely to have detected optical modulations and have >100 COUP counts than more massive stars (Figure 9a). Moreover measurement of P_{rot} through optical modulation may be impeded at the earliest stellar evolutionary stages due to high stochastic variability related to mass accretion. Compared to the “searched” sample, stars in the “modulated” samples appear to occupy the same area in the HR diagram and to span the full range of stellar masses and ages. This is confirmed by two-sided Kolmogorov-Smirnov (KS) tests that do not allow rejection of the null hypothesis that the distributions of masses and ages are drawn from the same parent population.

Figure 9a,b show the run of L_X and L_X/L_{bol} with stellar mass for the same samples. We observe that, respect to the “global” sample, stars in the “searched” sample, i.e. with optical rotation periods, have larger than average L_X and L_X/L_{bol} and this is confirmed with high significance by a statistical comparison of the distributions of $\log L_X$ and $\log L_X/L_{bol}$. This bias was noticed before (Flaccomio et al. 2003a; Stassun et al. 2004) and might be due to a positive correlation between coronal activity and presence of stellar spots responsible for the

⁷Note that we will not consider sources in class “ \neq ”. The simulations described in §4.2 indicate that most are likely to be spurious period detections.

modulation in the optical band. We note that the bias appears to be stronger in L_X/L_{bol} ; this could result because, given a fixed photometric precision, the probability of detecting an optical modulation depends on the contrast between spot coverage (likely related to L_X) and average optical luminosity. Within the “searched” sample there is a tendency to find more X-ray modulated stars at high L_X values or, equivalently, high count-rates. For example, within the 36 stars in the “searched” sample with $30.5 < \log L_X < 31$ ergs/s, about 20% (7 stars) are modulated while the same fraction for the 45 stars with $\log L_X < 29.5$ ergs/s is only 2% (1 star). This effect is likely a bias due to photons statistics: the more photons in our light curves the more easily we detect periodicity. The L_X/L_{bol} distributions of “searched” and “modulated” stars are instead statistically indistinguishable. Due to the bias in the “searched” sample however most of the “modulated” stars have high values of $L_X/L_{bol} \sim 10^{-3}$.

We investigated possible dependences of the periodicity detection fraction from an indicator of mass accretion, the equivalent width of the CaII ($\lambda = 8542\text{\AA}$) line, and from an indicator of disk presence, the $\Delta(I - K)$ excess, both reported by Hillenbrand (1997). Any such effect would indicate a difference in the spatial distribution of X-ray emitting plasma in the surroundings CTTS and WTTS. No striking trend in the modulation detection fraction was found. However, with both indicators, we found a hint (significance $\sim 1\%$) that stars with $P_X/P_{opt} \sim \frac{1}{2}$ preferentially are accreting and have disks.

Finally we have searched for correlations of the relative modulation amplitudes with mass, CaII, $\Delta(I - K)$, L_X , L_X/L_{bol} , P_X , P_X/P_{opt} , without finding any.

5. Discussion: The geometry of PMS X-ray emitting structures

5.1. Summary of main findings and astrophysical background

We have searched for rotational modulation of X-ray emission in a sample of 233 ONC stars. These are all stars with rotational period larger than 2 days known from optical photometric studies and with more than 100 counts collected in the COUP dataset. This sample spans the wide mass and age range of ONC members ($0.1 < M < 3 M_\odot$, $10^5 < t < 10^7$ yr). We reliably detect rotational modulation with amplitudes between 20% and 70% in 23 stars or $\sim 10\%$ of the searched sample. For 16 sources, the X-ray emission is modulated at periods very close to the optical rotational periods, while for the remaining 7 cases the X-ray period is about one half of the optical period. We further identify 86 stars where some evidence for modulation is found. Many, but likely not all, of these periodicities are spurious due to the difficulties in accounting for X-ray flares and other non-rotational variability. The

23 stars with rotation related modulation have higher than average X-ray luminosities with respect to stars in the searched sample, likely a bias due to the analysis. In all other respects they share the same physical properties – mass, age and accretion – of the searched sample. Based on these results and on previous finding summarized below, in the next subsection we discuss implications for the geometry of the X-ray emitting plasma on our young stellar systems.

The high temperatures and rapid variations of PMS X-ray emission, amply demonstrated in COUP lightcurves, implies that X-ray emitting plasma must be confined by magnetic fields and heated by violent magnetic reconnection events. In isolated, older, magnetically active stars, these magnetic fields are thought to be similar to those that are observed in the solar corona, mostly small-scale loops that connect spots of different magnetic polarity on the photosphere.

But the configuration of the confining magnetic field around young PMS stars might be more complicated, as these stars are often surrounded by circumstellar accretion disks. A variety of astrophysical models developed with a variety of motivations suggest that the PMS stellar magnetic field extends out 5 – 10 stellar radii to the inner edge of the disk and interacts strongly with disk material (e.g. Königl 1991; Calvet & Hartmann 1992; Collier Cameron & Campbell 1993; Shu et al. 1994). This results in funneling some disk material in an accretion flow, launching other disk material outward into jets and outflows, and locking the stellar rotation to corotate with the inner disk. There have been suggestions that, due to shear and instabilities, magnetic reconnection will occur in these long star-disk loops, producing X-ray emitting plasma (e.g. Hayashi et al. 1996; Shu et al. 1997; Montmerle et al. 2000; Isobe et al. 2003). However, the detailed properties of X-ray emission, together with extensive evidence for multipolar fields on PMS stellar surfaces, have generally supported a more standard stellar activity model as applied to older stars such as dMe flare and RS CVn systems (see reviews by Feigelson & Montmerle 1999; Favata & Micela 2003; Güdel 2004). Perhaps the first direct indication that the observed X-rays may sometimes arise from large-scale star-disk structures arises from detailed modeling of powerful flares observed during the COUP observation (Favata et al. 2005).

5.2. Implications of the X-ray rotational modulations

The detection of modulation of X-ray emission at periods related to the stellar rotation period in $\sim 10\%$ of COUP stars has three immediate implications:

1. The X-ray emitting structures are directly associated with the stellar surface. This

precludes the rarely considered model that both footpoints of the flaring magnetic loops reside in the shearing circumstellar disk (Romanova et al. 1998).

2. The X-ray emitting structures are not homogeneously distributed in longitude on the stellar surfaces. The amplitudes of the modulations seen in the 23 periodic COUP stars range from 20% to 70% (Table 2, column 13), indicating that the hemispheric brightness differences can reach roughly a factor of 2:1.
3. The bulk of the plasma emitting in the *Chandra* 0.5 – 8 keV band is confined in magnetic structures that, in order to undergo eclipse from the rotating star, may not extend at distances larger than $\sim R_\star$ from the stellar surface. This conclusion is not entirely inescapable if special geometries are considered. For example, eclipses could occur if the X-ray emission arises from the footpoints of corotating star-disk loops when the disk is viewed nearly edge-on. This and other similar possibilities we could think of seem unlikely to occur in 10% of otherwise ordinary PMS stars in the Orion Nebula Cluster. We thus view the detection of periodic X-ray modulations related to the optical rotation period to be a solid indication that in these stars the X-ray emitting structures responsible for the observed modulation are compact with characteristic lengths $l \lesssim R_\star$ or $l \ll R_\star$.

It seems likely that, due to the challenges of reliably detecting periodic modulations in COUP stars, more than 10% of the stars have intrinsic X-ray periodic modulations. Three types of stars will be missed by our analysis: stars with small X-ray periodic amplitudes compared to aperiodic variations such as Poisson noise and flares; stars with large-scale inhomogeneous X-ray structures viewed too close to their rotational axis for self-eclipsing to occur; and stars with several or many small-scale inhomogeneities. In this last case, some bright features emerge from eclipse as others enter eclipse, so the net rotational modulation has smaller amplitude than the smaller-scale spatial variations. This scenario of multiple X-ray hot spots near the surface is supported by our discovery of several COUP stars with $P_X = 0.5P_{opt}$, attributable to the eclipses and emergences of bright areas on opposing hemispheres. We thus conclude that *at least* 10% of COUP stars have large-scale structure in the longitude distribution of the X-ray emitting loops on scales less than a stellar radius.

Perhaps the most valuable inference that emerges from our findings concerns the enigma of ‘saturation’ in magnetically active stars. Our low mass modulated stars have very high levels of $\log L_X/L_{bol}$ (Figure 9b). Excluding one high mass star (COUP 1116, $M \sim 6M_\odot$) the median value is -3.05, basically the saturation level seen in magnetically active stars. At least for these stars, we can exclude one of the several suggested explanations for saturation (§1): it can not arise due to an uniformly filling of the stellar surface with X-ray emitting

plasma. A surface fully covered with X-ray loops would limit rotational modulation to a very low level. We note that, if we assume a solar-like picture for the X-ray emitting regions and their relation with stellar photospheres, our finding is in agreement with the existence on these stars of photospheric inhomogeneities similar to solar spots, as inferred from optical rotational modulation.

5.3. Comparison with the Sun

It is helpful to consider the Sun, the only star for which we have directly imaged longitudinal X-ray structures over many years. The astronomical and astrophysical similarities between the Sun and magnetically active stars has been well-documented (Schrijver & Zwaan 2000). It is important to keep in mind that the solar X-ray corona is certainly very different from that of our PMS stars. It is rotating much slower, has a much softer X-ray spectrum (even during flares), and is hugely less luminous. Latitude distributions of active regions may differ in PMS stars, and viewing orientations will be random rather than optimized for rotational eclipses.

The YOHKOH Soft X-ray Telescope (Tsuneta et al. 1991) has obtained an almost continuous time series of disk integrated solar fluxes comprising $\sim 150,000$ measurements in its AlMg band ($\sim 0.4 - 4$ keV) between 10 Nov 1991 and 21 Dec 2000 (both at solar maximum) and including one solar minimum around 1996-1997. Due to the SXT operating mode, times during the most energetic flares are automatically excluded from the time series. We have analyzed this dataset in a fashion similar to that performed on the ONC stars. We first divide the data into contiguous 81 day long segments, each comprising three solar rotation periods. The LNP analysis is then applied to each segment as described in §3 searching for periods between 2 and 81 days. Figure 10 shows the typical results for four segments. As with COUP stars, the panels show the X-ray lightcurves, LNP periodograms, and the lightcurves folded with the best period. On top of light curve we show YOHKOH images of the solar corona at corresponding times. In all the cases shown the periodograms and folded lightcurves refer to the lightly trimmed (“L”) lightcurves.

Our procedures succeed in retrieving the solar rotation period $P \simeq 27.3$ d in $\sim 75\%$ of the temporal segments. This is a much higher success rate than for the ONC sample. Three factors make period finding easier for the solar case: extremely strong signals; optimal inclination of the rotation axis; and flares (those not automatically excluded from the time series) with durations much shorter than the rotation period. Modulation amplitudes computed from the folded lightcurves, range between 20% and 60% (median $\sim 0.35\%$), similar to the rotationally modulated COUP stars. There might be a tendency to have slightly

lower relative amplitudes at solar maximum rather than at minimum. The shape of the light curves vary significantly between segments depending on the configuration of active regions; broadly speaking they are similar to the ones we observed in our PMS stellar sample.

From this first comparison between stellar COUP data and the solar YOHKOH data we conclude that, although in PMS stars plasma emission measures and temperatures are tremendously higher, the degree of longitudinal inhomogeneity in the X-ray emitting regions are qualitatively similar. It is thus reasonable to view both the 2-dimensional surface distribution – dominated by one or a few active regions – and the 3-dimensional distribution – dominated by emission close to the stellar surface – of X-ray emission in the Sun to be similar to that in PMS stars.

6. Summary

We have searched for rotational modulation of X-ray emission in a sample of 233 young PMS stars in the Orion Nebula Cluster. The study was made possible by the *Chandra Orion Ultradeep Project* which obtained an 850ks long ACIS observation of the region during a time span of 13.2 days. In order to check that the observed X-ray modulation is related to stellar rotation, this work focused on a selected sample of stars with known rotation period.

Periodicity in binned light-curves was searched with the Lomb Normalized Periodogram method. The analysis was performed both on unfiltered lightcurve and on lightcurves that were first trimmed to remove large flares. False alarm probabilities were estimated so as to take into account the presence of non-rotational short-term (< 8 hour) variability such as flares; because of non-rotational variability with longer timescales these FAPs remain indicative. We thus verified our analysis technique using extensive numerical simulations.

We reliably establish the presence of X-ray rotational modulation in 23 stars, 10% of the searched sample and the largest sample of stars of any class in which X-ray rotational modulation has been observed to date. For 86 additional stars in the searched sample the detection of rotational modulation is less reliable. Within the 23 reliable detections relative amplitudes range from 20% to 70% and periods between 2 and 12 days. In 16 cases the X-ray modulation period is similar to the stellar rotation period, while in seven cases it is about half that value. The data suggest that X-ray periods are on average 5-10% longer than either P_{opt} or $0.5P_{opt}$.

Comparing the stellar properties of the modulated sample to those of the searched sample, we find that the two sample are indistinguishable with respect to mass, age and accretion disk properties. X-ray modulation is however detected preferentially in bright X-

ray sources. We understand this as a selection effect. The data also suggest, albeit with low significance, that stars with $P_X \sim 0.5 \times P_{opt}$ are preferentially active accretors, according to the CaII line EW, and posses disks, according to the K band excess.

Our main conclusions, referred to the stars that show modulation, are:

1. X-ray emitting plasma is inhomogeneously distributed in longitude. A comparison with solar data suggests a similar degree of inhomogeneity.
2. Saturation of activity, $L_X/L_{bol} \sim 10^{-3}$, is not due to the filling of the stellar surface with active region.
3. Dominant emitting structures are likely compact with sizes $\lesssim R_\star$.

The last conclusion may seem in contrast with that of Favata et al. (2005) based on the analysis of the decay phase of the most luminous flares observed during the COUP observation. Favata et al. (2005) find that a number of large flares can be modelled only by assuming very long magnetic loops ($5 - 20 R_\star$). It is not yet clear how common these large loops structures are. It is conceivable that long-lived compact structures are the most common and that they coexist with extended ones that may become prominent during flares.

The authors are grateful to K. Stassun, S. Shang and S. Orlando for useful discussion. COUP is supported by *Chandra* Guest Observer grant SAO GO3-4009A (E. Feigelson, PI). E.F., G.M. and S.S. acknowledge financial support from the *Ministero dell’Istruzione dell’Università e della Ricerca*. E.D.F. is also supported by ACIS Team contract NAS8-38252.

A. Simulations of COUP X-ray lightcurves

This Appendix describes the development of simulated X-ray lightcurves to test the performance of our analysis techniques in datasets suffering the realistic complexities seen in COUP ONC X-ray lightcurves. These include repeated high-amplitude flaring, longer-timescale aperiodic variations, gaps in the exposure due to the *Chandra* orbital perigees, and Poissonian noise. Other currently unknown sources of variability might also be present. We focus much attention on the effect of flares on the period detection procedures. Simulating realistic light curves is not straightforward because it requires the knowledge of several input quantities that are at present not well constrained, such as the flare frequency, distributions of flare amplitudes and durations, the relative contribution of flares and “quiescent” emission, if at all present. These issues are studied for a small sample of $1 M_{\odot}$ COUP stars by Wolk et al. (2005), but have not yet been characterized for the full COUP sample.

We therefore introduce a model of the stellar X-ray emission that is simple enough to be described with few parameters, but still yields lightcurves that qualitatively resemble observed ones. The model lightcurves are made exclusively out of a distribution of flares based on the well-studied idea that even stellar “quiescent” emission arises from the superposition of many microflares (Kashyap et al. 2002, and references therein). Forthcoming COUP studies will tackle this issue in greater detail. Here, we introduce this model exclusively as a tool to produce useful lightcurves.

A.1. Construction of simulated lightcurves

The following procedure was followed for creating unmodulated lightcurves⁸:

1. Generate a specified number, NF , of random flare start times, uniformly distributed between $t_0 - 3\tau_{fl}$ and t_1 where t_0, t_1 are the start and end times of our COUP observation and τ_{fl} is a specified decay timescale for flares.
2. Assign to each of the NF flares an intrinsic amplitude, C_0 or total number of counts, obtained from the probability distribution $\frac{dn}{dC_0} \propto C_0^{-\alpha}$ where α is a specified powerlaw index of the flare intensity distribution. We find (see below) that the observed data is

⁸Throughout these simulation we will neglect background contributions to the light curves. This is justified by the relative unimportance of background for the majority of COUP sources (Getman et al. 2005), implying that the noise properties of real background-subtracted lightcurves are very similar to those of background-free simulated lightcurves.

best reproduced by α larger than two. To avoid an energy divergence of small flares we arbitrarily adopt a lower limit $C_0 > C_{min} = 1$ of flare intensities⁹.

3. Compute the observed amplitude C for each flare, randomly taken from a Poisson distribution with mean C_0 .
4. Simulate C photons arrival times for each flare, assuming an instantaneous rise and an exponential decay with a decay time τ_{fl} .
5. Merge the arrival times for each flare so to generate the simulated light curve.
6. Filter out simulated events that fall outside the Good Time Intervals of the COUP observation (i.e. in the gaps due to the *Chandra* satellite orbital perigee).

Having fixed C_{min} , the free parameters in the model are α , the steepness of the flare amplitude distribution, NF , the number of flares, and τ_{fl} , the flare decay time. We consider two values of τ_{fl} , 5 hr and 8 hr, consistent with the typical flare durations seen in COUP lightcurves. Setting NF is equivalent to setting the total counts for the source. We examined lightcurves produced with values of α ranging between 2.0 and 3.0. The flatter $\alpha=2.0$ distribution produces lightcurves with far too many bright flares compared to typical COUP lightcurves, while $\alpha=3.0$ clearly results in too few bright flares. Figure 12 shows six examples of simulated light curves.

In order to simulate rotational modulation, we modify the distribution from which flare start times are drawn (step 1) from a constant distribution to a sinusoidal one with a given input period (P_{in}) and amplitude (Amp). We then apply our period searching methodology (§3) to all simulated lightcurves, including attempts to trim flares, calculate LNPs, estimate FAPs, and select significant results according to various criteria.

We initially ran these simulations choosing the input parameters from the following grid: α = 2.0 to 3.0 in 0.25 steps, NF = 500, 1000 and 2000, Amp = 0% to 100% in 20% steps. P_{in} were chosen equal to the optically determined rotation periods of the 233 stars in our main sample, repeated five times so as to have, for each choice of the other parameters, 1165 simulated light curves with P_{in} distributed as P_{rot} . The value of α was constrained using two simple strategies to compare real and simulated lightcurves with a similar number of counts: visual examination of simulated and real lightcurves, and comparison of the standard deviation of the count rates in the binned lightcurves. Both of these qualitative comparisons indicate that α between 2.25 and 2.5 gives light curves that most resemble the observed ones.

⁹Corresponding to a minimum flare energy $\sim 5 \times 10^{32}$ ergs.

With these choices of α , the NF (number of flares) that reproduces the median observed number of counts in our “searched” sample (~ 2300) is between 500 and 1000. Simulations using these parameters, with and without periodic modulations applied, were then used to study the performance of our period finding method.

A.2. Results for simulated unmodulated COUP sources

Simulations with $Amp = 0.0$ are valuable to testing the false alarm probabilities which may lead to spurious period detections. Figure 13 shows, in the same format of Figure 6 with actual COUP data, the distributions of $\log P_{out}/P_{in}$, for the three selections of “significant” periods (“ $N + L + H$ ”, “ N ”, “ $N \cdot L \cdot H$ ”) and for our chosen ranges of model input parameters. The histograms are normalized to yield the expected distributions for our “searched” sample. Since the simulated lightcurves are not modulated, there is no relation between input and output period. The shape of the simulated distributions therefore solely reflects the distribution of *spurious* detected X-ray periods with respect to the input optical stellar rotation periods. The distributions show that using a realistic model of the X-ray emission from ONC stars:

1. Detection of spurious periods due to our failure to properly account and/or remove flares, cannot explain the observed sharp peaks in the observed P_X/P_{opt} histogram.
2. Flares can account for most or all of the X-ray periods that do not fall within these peaks and that are therefore unrelated to optical periods. It is also apparent that the number of spurious periods found in these unmodulated lightcurves is largest when accepting periods that have $FAP < 0.1\%$ in any of the three analyzed light curves (the “ $N + L + H$ ” sample) and lowest when accepting only periods with $FAP < 0.1\%$ in all three analyses (the “ $N \cdot L \cdot H$ ” sample).

A.3. Results for simulated modulated COUP sources

Figure 14 shows in the same format results for simulated lightcurves with a small, 20%, intrinsic modulation. Success in retrieving the input periods would be indicated by a narrow peak at $\log P_{out}/P_{in} = 0$ containing the largest possible fraction of the 233 input sources. We find that most periods can be retrieved using our method, most cleanly in the “ $N \cdot L \cdot H$ ” selection that includes heavy trimming of flares. Tails of spurious periods are found. Note that it is easier to retrieve the input periods for the larger value of α (i.e. when large flares

are less frequent) and for the larger number of flares, NF (i.e. when the total source counts are higher). Larger relative modulation amplitudes (not shown) also results in higher success rates. Several other indications can be read from Figure 14 as well as from similar ones for the other amplitudes:

1. The uncertainties in the derived period, i.e. the width of the peak in the P_{out}/P_{in} ratio histograms are of the same order of the width in the corresponding plot based on real COUP data.
2. Aliases of the input periods are *not* seen in the simulations, such as the $P_X = 0.5P_{opt}$ secondary peak clearly seen in the real COUP data. We only obtain a peak at $P_{out}/P_{in} = 1$ and a scattered tail in the range $0.2 < P_X/P_{opt} < 5$.
3. No systematic shift between P_{out} and P_{in} is observed.
4. Short periods are determined more precisely (not shown). This occurs because more modulation periods are covered by the observation. It might also explain the smaller width of the $P_X/P_{opt} \sim 0.5$ peak in Figure 6.
5. Periods from ~ 1 day and ~ 13 days can be retrieved, confirming the results of the purely periodic simulations (§3).

REFERENCES

Calvet, N., & Hartmann, L. 1992, *ApJ*, 386, 239

Carpenter, J. M., Hillenbrand, L. A., & Skrutskie, M. F. 2001, *AJ*, 121, 3160

Collier Cameron, A., & Campbell, C. G. 1993, *A&A*, 274, 309

Damiani, F., & Micela, G. 1995, *ApJ*, 446, 341

Drake, J. J., Peres, G., Orlando, S., Laming, J. M., & Maggio, A. 2000, *ApJ*, 545, 1074

Favata, F. & Schmitt, J. H. M. M. 1999, *A&A*, 350, 900

Favata, F., & Micela, G. 2003, *Space Science Reviews*, 108, 577

Favata, F., et al. , 2005, *ApJS*, submittted

Feigelson, E. D., & Montmerle, T. 1999, *ARA&A*, 37, 363

Flaccomio, E., Damiani, F., Micela, G., et al. 2003, *ApJ*, 582, 398

Flaccomio, E., Micela, G., & Sciortino, S. 2003, *A&A*, 397, 611

Getman, K. V., Flaccomio, E., Bross, P. S. et al. 2005 *ApJS*, this issue

Grosso, N., et al. , 2005, *ApJS*, this issue

Guedel, M., Schmitt, J. H. M. M., Benz, A. O., & Elias, N. M. 1995, *A&A*, 301, 201

Güdel, M. 2004, *A&A Rev.*, 12, 71

Hayashi, M. R., Shibata, K., & Matsumoto, R. 1996, *ApJ*, 468, L37

Herbst, W., Rhode, K. L., Hillenbrand, L. A., & Curran, G. 2000, *AJ*, 119, 261

Herbst, W., Bailer-Jones, C. A. L., Mundt, R., Meisenheimer, K., & Wackermann, R. 2002, *A&A*, 396, 513

Hillenbrand, L. A. 1997, *AJ*, 113, 1733

Hussain et al., *ApJ*, in press

Kastner, J. H., Huenemoerder, D. P., Schulz, N. S., Canizares, C. R., & Weintraub, D. A. 2002, *ApJ*, 567, 434

Isobe, H., Shibata, K., Yokoyama, T., & Imanishi, K. 2003, *PASJ*, 55, 967

Jardine, M., Wood, K., Collier Cameron, A., Donati, J.-F., & Mackay, D. H. 2002, NMRAS, 336, 1364

Jones, B. F., & Walker, M. F. 1988, AJ, 95, 1755

Kashyap, V. L., Drake, J. J., Güdel, M., & Audard, M. 2002, ApJ, 580, 1118

Königl, A. 1991, ApJ, 370, L39

Lafler, J., & Kinman, T. D. 1965, ApJS, 11, 216

Lucas, P. W. & Roche, P. F. 2000, MNRAS, 314, 858

Marino, A., Micela, G., Peres, G., & Sciortino, S. 2003, A&A, 407, L63

Montmerle, T., Grosso, N., Tsuboi, Y., & Koyama, K. 2000, ApJ, 532, 1097

Muzerolle, J., Calvet, N., & Hartmann, L. 2001, ApJ, 550, 944

Orlando, S., Peres, G., & Reale, F. 2001, ApJ, 560, 499

Pizzolato, N., Maggio, A., Micela, G., Sciortino, S., & Ventura, P. 2003, A&A, 397, 147

Preibish, T., et al. , 2005, ApJS, submitted

Romanova, M. M., Ustyugova, G. V., Koldoba, A. V., Chechetkin, V. M., & Lovelace, R. V. E. 1998, ApJ, 500, 703

Scargle, J. D. 1982, ApJ, 263, 835

Schrijver, C. J., & Zwaan, C. 2000, Solar and stellar magnetic activity, Cambridge University Press

Schuster, A. 1898, Terr. Mag., 3, 13

Shu, F., Najita, J., Ostriker, E., Wilkin, F., Ruden, S., & Lizano, S. 1994, ApJ, 429, 781

Shu, F. H., Shang, H., Glassgold, A. E., & Lee, T. 1997, Science, 277, 1475

Stassun, K. G., Mathieu, R. D., Mazeh, T., & Vrba, F. J. 1999, AJ, 117, 2941

Stassun, K. G., Ardila, D. R., Barsony, M., Basri, G., & Mathieu, R. D. 2004, AJ, 127, 3537

Stelzer, B., & Schmitt, J. H. M. M. 2004, A&A, 418, 687

Stelzer, B., et al. , 2005, ApJS, submitted

Tsuneta, S., et al. 1991, Sol. Phys., 136, 37

Wolk, S., et al. , 2005, ApJS, submitted

Schmitt, J. H. M. M., Robrade, J., Ness, J.-U., Favata, F., Stelzer, B. 2005, A&Ain press

Table 1. Data

COUP	Cts ^a	Id.	P_{opt} [d]	Ref. ^b	Mass [M_{\odot}]	log Age [yr]	log L _X [ergs/s]	log L _X /L _{bol}	EW(CaII)	Mod.Fl. ^c
6	1887	40	9.81	H	0.23	6.3	29.8	-3.2	0.0	LH
17	1083	63	4.10	cs	0.90	6.1	30.1	-3.8	1.9	-
20	382	70	1.50	H	0.16	5.3	29.4	-3.7	0.0	†
23	55449	75	3.45	h	2.17	6.2	31.3	-3.2	–	–
27	5948	77	1.50 ^d	cshH	0.53	6.2	30.3	-3.1	1.8	†
28	20863	81	4.41	H	0.53	6.0	30.9	-2.6	1.6	L
29	2287	83	7.72	sh	0.33	6.1	30.0	-3.3	-9.2	-
30	169	84	2.45	H	0.25	6.4	28.8	-4.1	0.0	-
41	574	98	2.34	H	0.21	6.0	29.3	-3.7	0.0	-
47	837	106	1.70	H	0.27	5.6	29.5	-3.8	1.5	†

Note. — Sample rows: the full table is available in the electronic edition of ApJ. Explanation of columns: (1) COUP source number; (2) net, background subtracted, ACIS counts; (3) optical source identification (Hillenbrand 1997; Herbst et al. 2002); (4) rotation period; (5) reference for the rotation period; (6) stellar mass; (7) log stellar age; (8) log L_X; (9) log L_X/L_{bol}; (10) CaII line equivalent width; (11) X-ray modulation flag.

^aNet photons collected during the 850ksec COUP observation in the source extraction area, including from 1% to 96% of the source point spread function ($\sim 90\%$ for most sources; Getman et al. 2005).

^bReference for P_{opt} : H=Herbst et al. (2002), h=Herbst et al. (2000), s=Stassun et al. (1999), c=Carpenter et al. (2001), U=Herbst (unpublished)

^cIndicates filtered light curves (N,L or H) for which the LNP analysis yielded FAP<0.1%. A † indicates that the periodogram analysis was not performed because either $P_{opt} < 2.0$ d or Cts < 100.

^dother period: 2.99(c)

Table 2. Results of the period analysis – “ $N \cdot L \cdot H$ ” sample

COUP	Cts ^a	Id.	P_{opt}	Ref. ^b	P_X^N	FAP	P_X^L	FAP^L	P_X^H	FAP^H	B	Amp.	Class
62	9294	123	6.63	s	8.13	0.06	9.09	0.00	11.51	0.03	L	0.72	1
131	9038	187	14.41	H	7.92	0.01	7.70	0.01	1.97	0.01	N	0.71	$\frac{1}{2}$
139	6094	192	9.04	sH	4.87	0.00	4.91	0.00	4.91	0.00	N	0.50	$\frac{1}{2}$
161	2428	211	5.46	sH	5.71	0.02	5.92	0.04	5.79	0.01	H	0.18	1
174	2810	222	5.17	shH	4.72	0.03	4.66	0.00	4.68	0.00	H	0.33	1
226	2676	258	10.98	cH	12.10	0.01	11.91	0.01	10.66	0.05	N	0.58	1
250	497	278	6.76	H	6.39	0.00	6.82	0.00	6.71	0.00	H	0.53	1
271	189	292	5.11	c	2.68	0.04	2.33	0.01	2.33	0.00	H	0.66	\neq
292	1580	–	7.83	c	10.39	0.00	10.00	0.00	9.83	0.00	L	0.61	1
413	3204	362	2.73	hH	6.79	0.06	6.72	0.01	6.09	0.02	L	0.47	\neq
454	17125	373	9.81	H	3.91	0.01	3.92	0.01	3.99	0.05	N	0.53	\neq
612	2305	435a	10.33	c	2.98	0.02	3.02	0.01	3.03	0.00	H	0.20	\neq
697	5984	470	10.70	h	9.62	0.00	9.93	0.00	10.22	0.00	H	0.38	1
1023	4852	9250	2.27	H	12.18	0.03	11.92	0.03	11.63	0.02	H	0.26	\neq
1070	4733	634	5.38	H	3.53	0.05	3.61	0.01	3.61	0.00	H	0.28	\neq
1116	52865	660	6.15	h	6.64	0.02	6.64	0.02	6.64	0.02	H	0.26	1
1141	874	9280	7.92	H	4.12	0.02	4.18	0.01	4.20	0.01	L	0.45	$\frac{1}{2}$
1161	9270	690	3.90	H	3.43	0.02	9.53	0.00	9.83	0.00	L	0.46	\neq
1216	637	721	2.45	h	6.55	0.05	6.76	0.04	6.63	0.08	L	0.49	\neq
1233	1056	727	6.03	h	8.40	0.01	8.20	0.00	8.20	0.04	L	0.58	1
1248	14567	733	3.28	sH	6.16	0.03	6.15	0.03	6.15	0.06	L	0.36	\neq
1335	5466	782	10.22	c	5.69	0.03	5.55	0.02	5.56	0.00	H	0.33	$\frac{1}{2}$
1355	5878	798	10.36	H	11.96	0.01	12.14	0.01	5.19	0.07	L	0.47	1
1382	10217	811a	11.10	h	5.61	0.00	5.61	0.00	5.63	0.00	H	0.25	$\frac{1}{2}$
1384	25433	813	2.85	cshH	2.79	0.08	2.87	0.06	2.87	0.06	H	0.44	1
1398	3037	823	9.00	hH	10.79	0.01	10.31	0.00	9.94	0.00	L	0.61	1
1421	6370	836	12.20	h	4.38	0.05	4.39	0.02	4.39	0.04	L	0.26	\neq
1423	3553	838	7.75	H	6.88	0.06	6.87	0.01	6.85	0.00	H	0.29	\neq
1429	5527	839	7.52	hH	8.22	0.01	8.09	0.00	8.04	0.00	L	0.30	1
1448	3304	860	6.33	cshH	7.82	0.06	7.89	0.00	7.97	0.00	H	0.30	1
1463	8214	867	10.66	H	11.20	0.09	3.95	0.10	10.87	0.07	H	0.34	1
1500	4438	892	8.56	hH	10.40	0.00	10.43	0.00	10.90	0.00	L	0.50	1
1570	4146	962	9.56	cH	4.99	0.00	4.97	0.00	4.92	0.01	L	0.63	$\frac{1}{2}$
1590	1190	982	7.10	c	3.59	0.02	3.62	0.01	3.49	0.01	L	0.50	$\frac{1}{2}$

Note. — Explanation of columns: (1) COUP source number; (2) net, background subtracted, ACIS counts; (3) optical source identification (Hillenbrand 1997; Herbst et al. 2002); (4) rotation period; (5) reference for the rotation period; (6, 8, 10) best X-ray period from the “N”, “L” and “H” analyses; (7, 9, 11) FAPs for the best X-ray periods in “N”, “L” and “H” analyses; (12) analysis that yielded the lowest FAP; (13) relative amplitude of the modulation computed from the averaged folded lightcurve as $(\max - \min) / (\max + \min)$; (14) source class according to P_X / P_{opt} .

^aNet photons collected during the 850ksec COUP observation in the source extraction area, including from 1% to 96% of the source point spread function ($\sim 90\%$ for most sources; Getman et al. 2005).

^bReference for P_{opt} : H=Herbst et al. (2002), h=Herbst et al. (2000), s=Stassun et al. (1999), c=Carpenter et al. (2001)

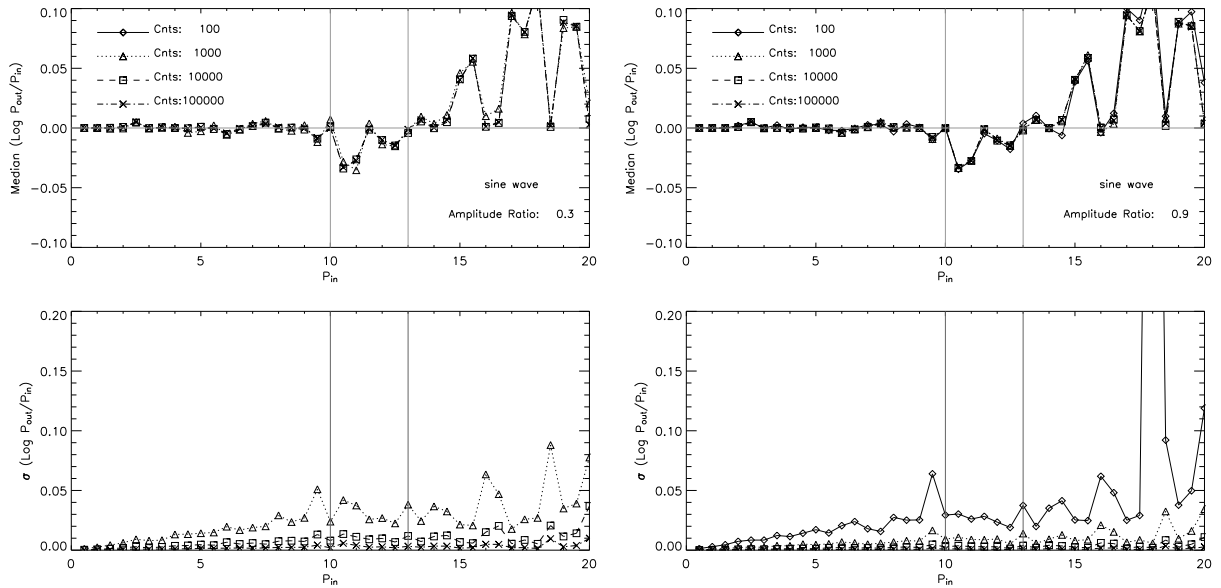


Fig. 1.— Results of simulations of purely periodic sinusoidal light curves for relative modulation amplitudes of 30% (left) and 90% (right). Upper panel: \log median P_{in}/P_{out} , as a function of P_{in} ; P_{in} is the input period for the simulation and P_{out} is the period corresponding to the main peak in the resulting periodogram. Each point is the result of 100 simulated sinusoidal light curves with counts ranging from 100 to 100000, as indicated in the label. Vertical lines indicate periods of 10 and 13 days, i.e. the exposure time and the total length of our observation including gaps. Lower panels: 1σ scatter of the 100 simulation around the median for the same simulations.

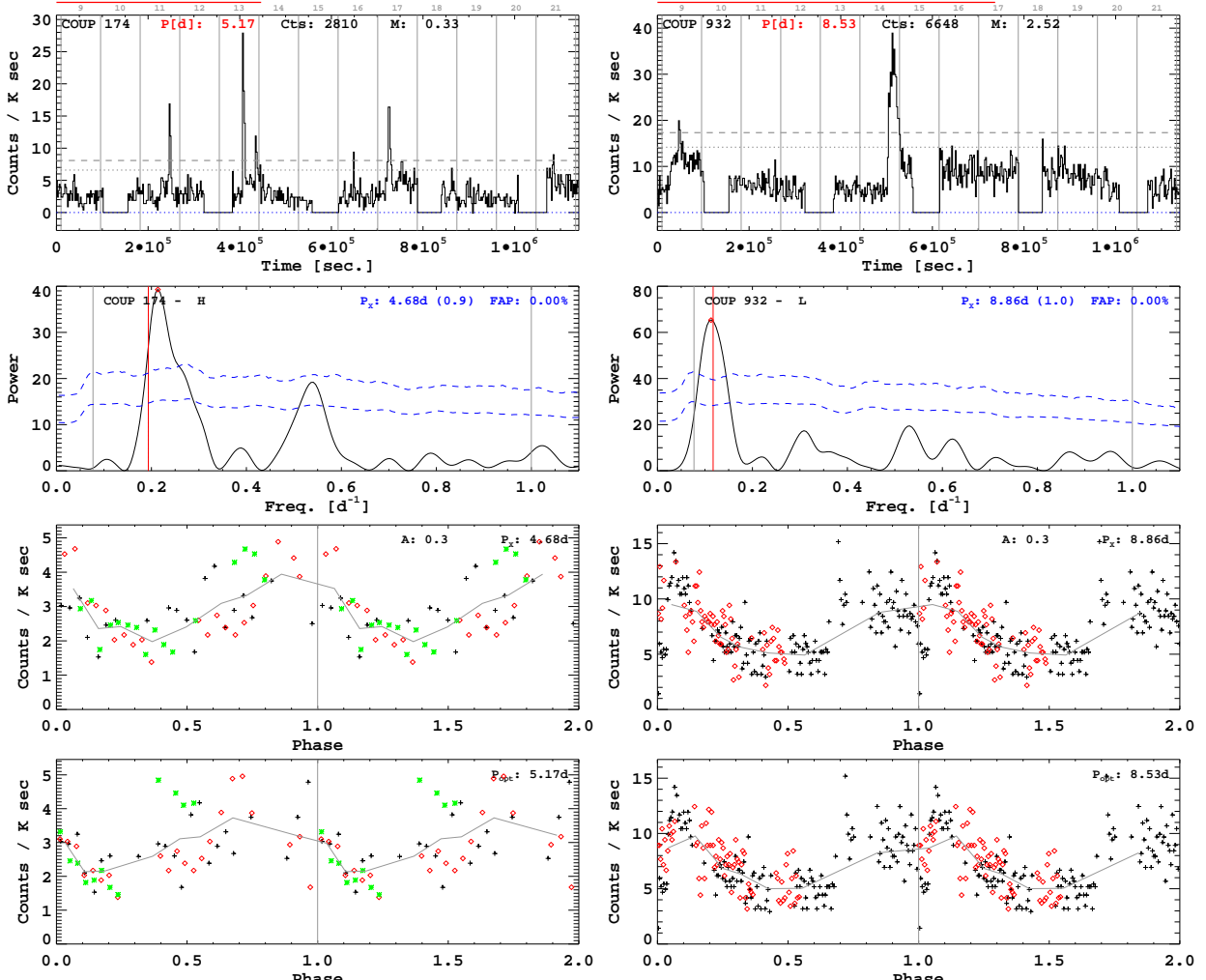


Fig. 2.— Upper panels: light curves for two sources (COUP 174 and COUP 932) for which the modulation analysis yielded X-ray periods similar to optically determined stellar rotation periods. Background subtracted count rates in 2000s bins are plotted versus the time since the beginning of the observation. UT dates (in January 2003) are given above the plot, between gray vertical lines indicating UT midnights. Source number, optical periods, extracted net counts and stellar mass are given in the upper part of the plot. The red horizontal segment above lightcurves indicates the length of one rotation period. The dashed and dotted horizontal lines indicate count-rate thresholds used for “light trimming” and “heavy trimming” respectively. Second row of panels: Lomb normalized periodograms for the light curves filtered so as to minimize the FAP. The filtering method (“N” none, “L” light trimming, “H” heavy trimming) is given next to the source id in the upper right corner. The red vertical line indicates the frequency corresponding to the optical rotation period. The two dashed curves indicate 1% and 0.1% FAP thresholds (see text). The most likely X-ray period is reported in the upper right corner (with in parenthesis the ratio P_X/P_{opt}) along with the FAP. Third row: light curves folded with the most likely X-ray period, reported in the upper right corner along with the relative modulation amplitude. Different symbols and colors indicate data-points belonging to different modulation cycles. The solid gray line indicate the average count-rate as a function of phase. Fourth row: light curves folded with the second most likely X-ray period, reported in the upper right corner along with the relative modulation amplitude. Different symbols and colors indicate data-points belonging to different modulation cycles. The solid gray line indicate the average count-rate as a function of phase.

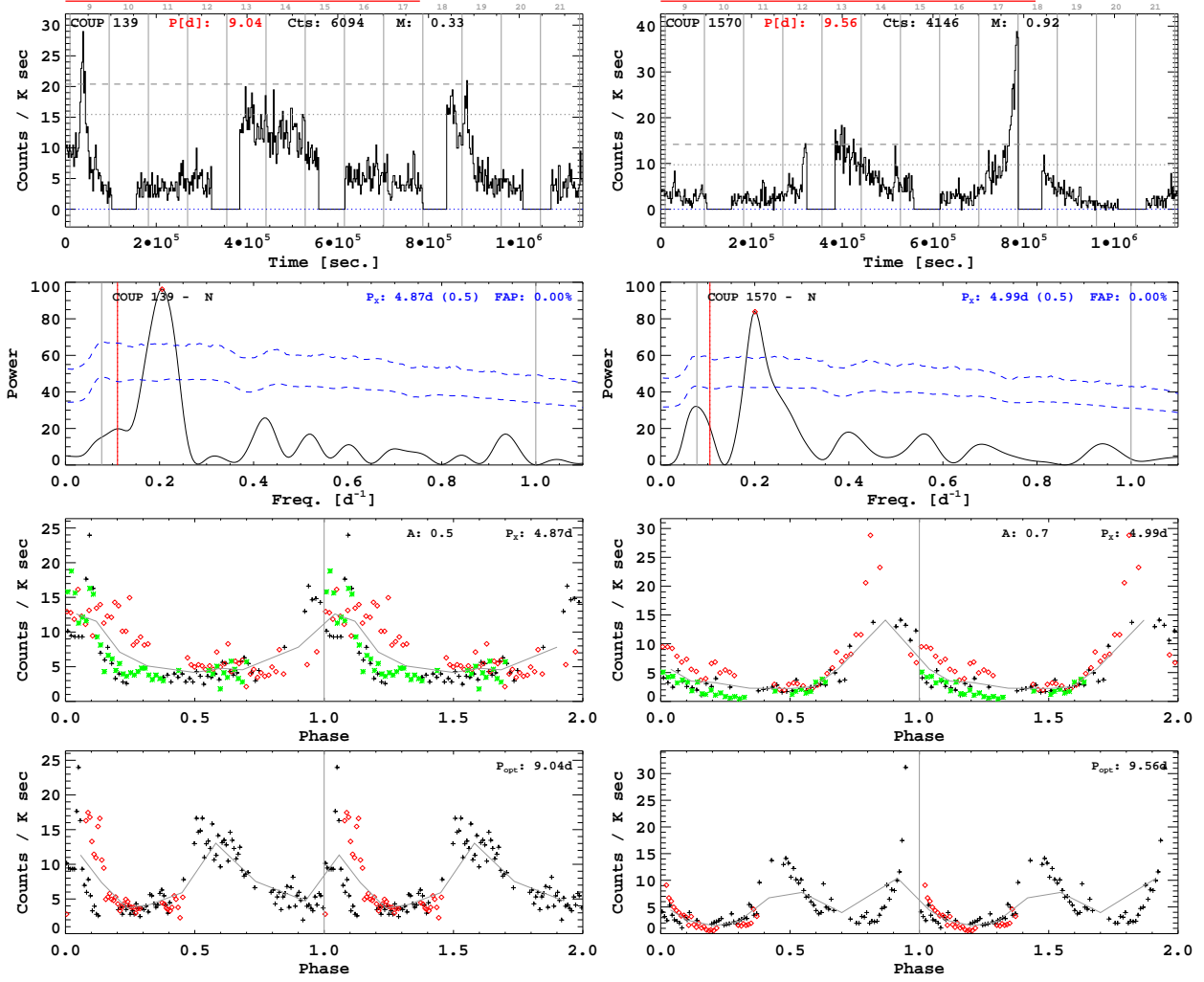


Fig. 3.— Same as figure 2 for two sources for which the most likely X-ray period is half the optical period. Note however that for the source on the left (COUP 139) a not significant peak is present at the optical period. Applying the “H” filter, the peak at $P \sim 4.9$ d remains predominant but the FAP of this secondary peak drops to 0.7%.

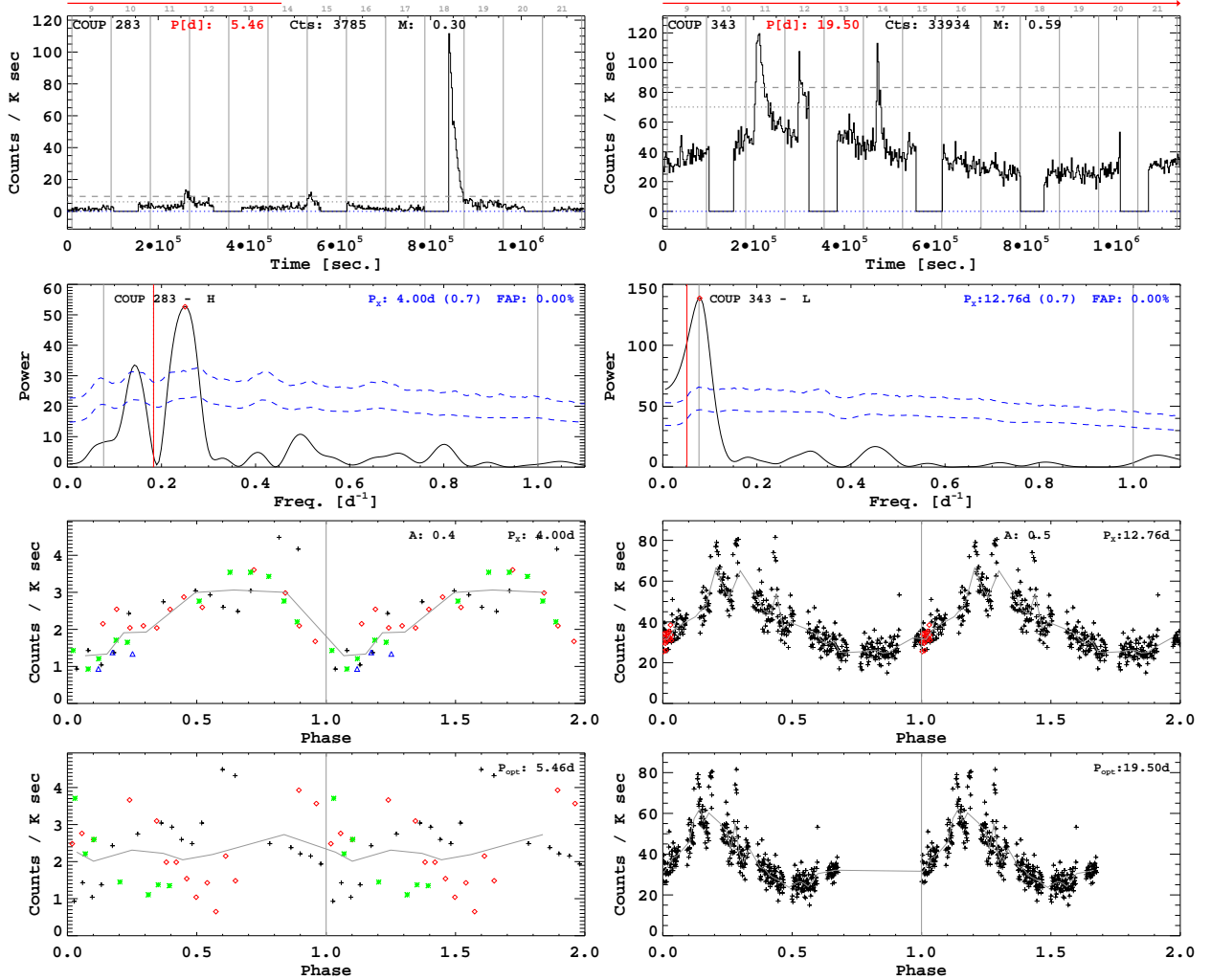


Fig. 4.— Same as figure 2 for two sources for which the most likely X-ray periods is apparently unrelated to the optical one.

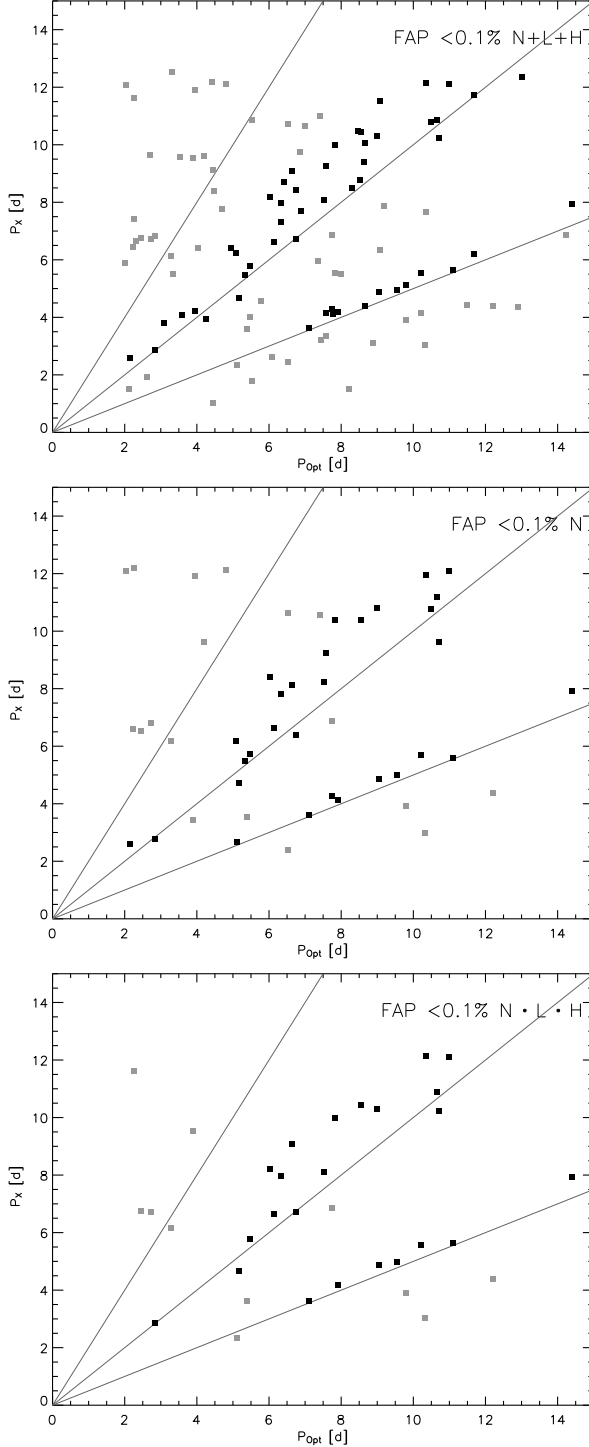


Fig. 5.— Scatter plot of the optical vs. X-ray periods. The three panels refer to three different source samples: (Top) “ $N + L + H$ ” with $\text{FAP} < 0.1\%$ in at least one of the filtered lightcurves; (middle) “ N ” with $\text{FAP} < 0.1\%$ in the non-filtered lightcurve; (Bottom) “ $N \cdot L \cdot H$ ” with $\text{FAP} < 0.1\%$ in all three filters. Darker dots indicate sources with $P_X \sim P_{\text{opt}}$ or $P_X \sim \frac{1}{2}P_{\text{opt}}$, i.e. those lying in the two main peaks in the histograms in Figure 6; lines indicate loci where $P_X = [\frac{1}{2}, 1, 2]P_{\text{opt}}$.

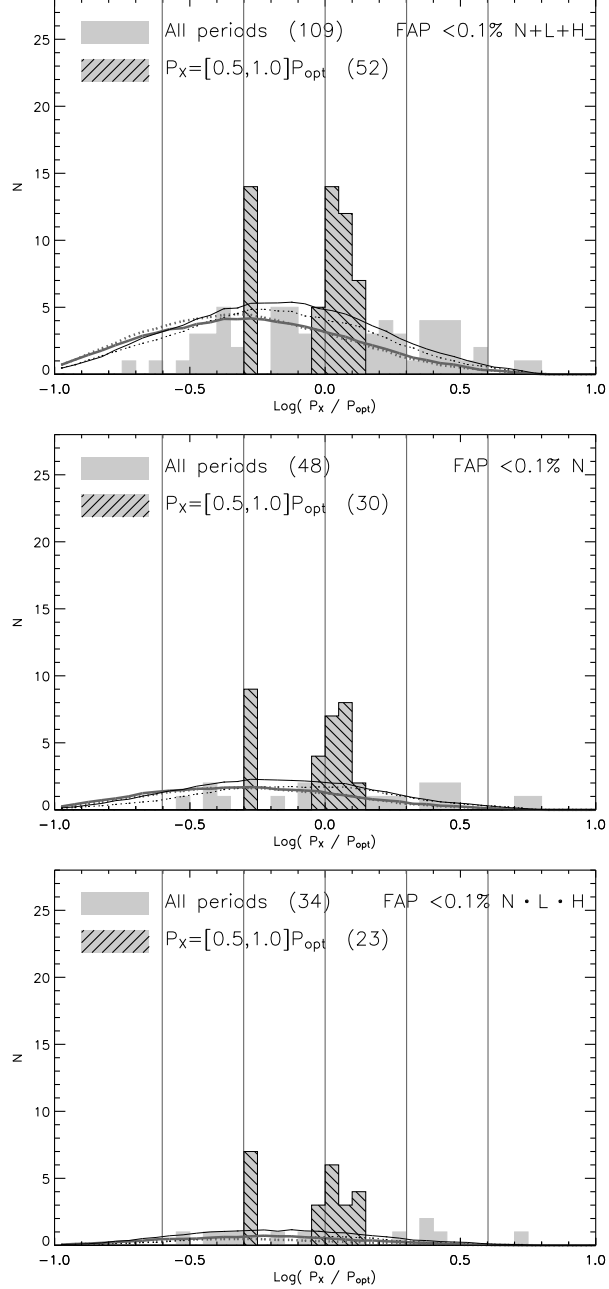


Fig. 6.— Distribution of the logarithm of the ratio between X-ray and optically determined periods for X-ray periods with FAP < 0.1% and three different choices of light curve filtering strategy as in Figure 5. Also shown (curves) are distributions resulting from the simulation of unmodulated flaring lightcurves (see Figure 13). Vertical lines indicate ratios of 1/4, 1/2, 1, 2 and 4.

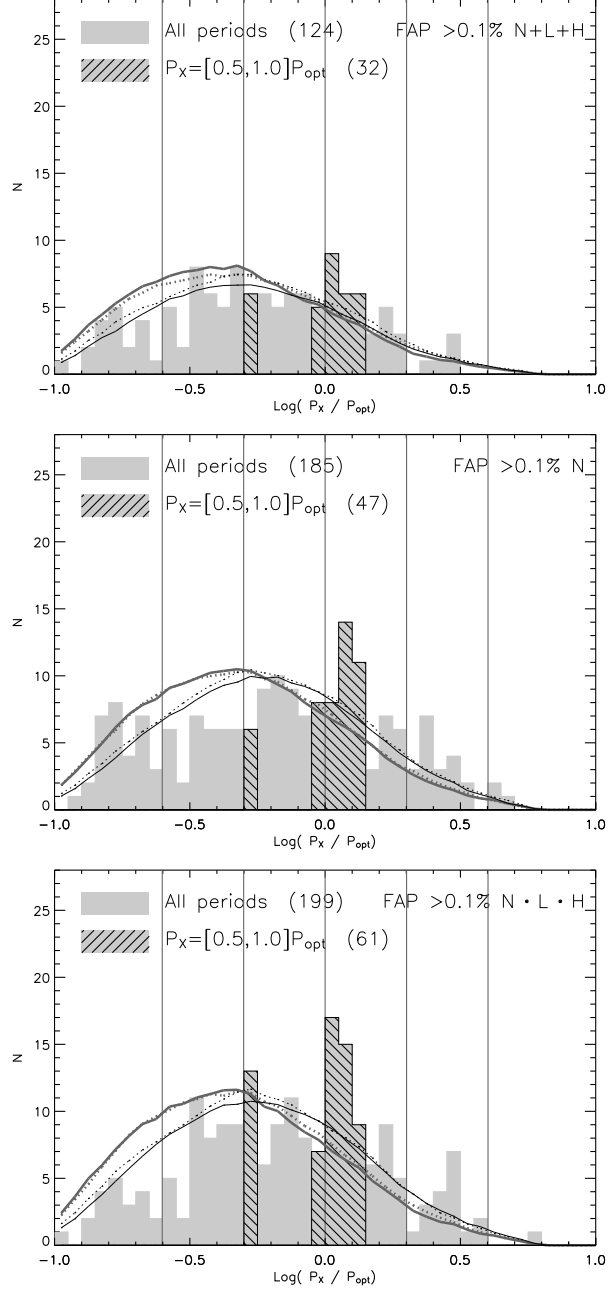


Fig. 7.— Distribution of X-ray and optical periods, as in Fig. 6, for COUP sources without significant periodic signals (FAP> 0.1%). Note that the peaks present in the previous figure have here largely disappeared.

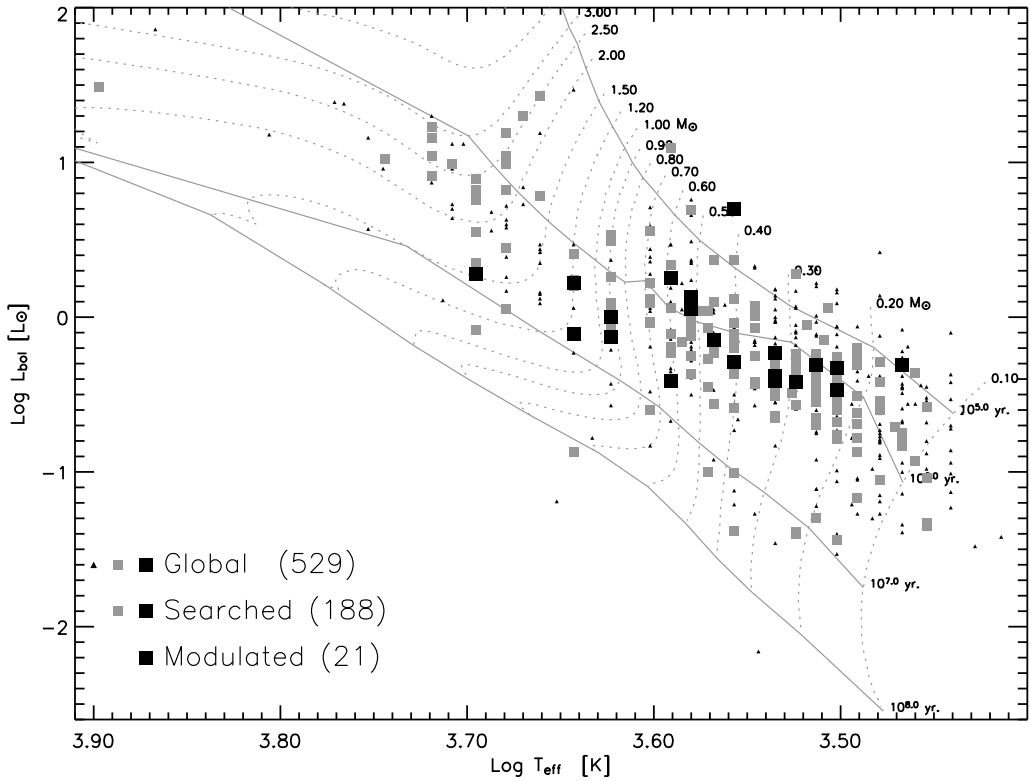


Fig. 8.— HR diagram for all COUP sources with >100 ACIS counts (“global”), for the sample for which we performed the period analysis (“searched”) and for the subsample of this latter for which we found X-ray periods with $\text{FAP} < 0.1\%$ (“modulated”).

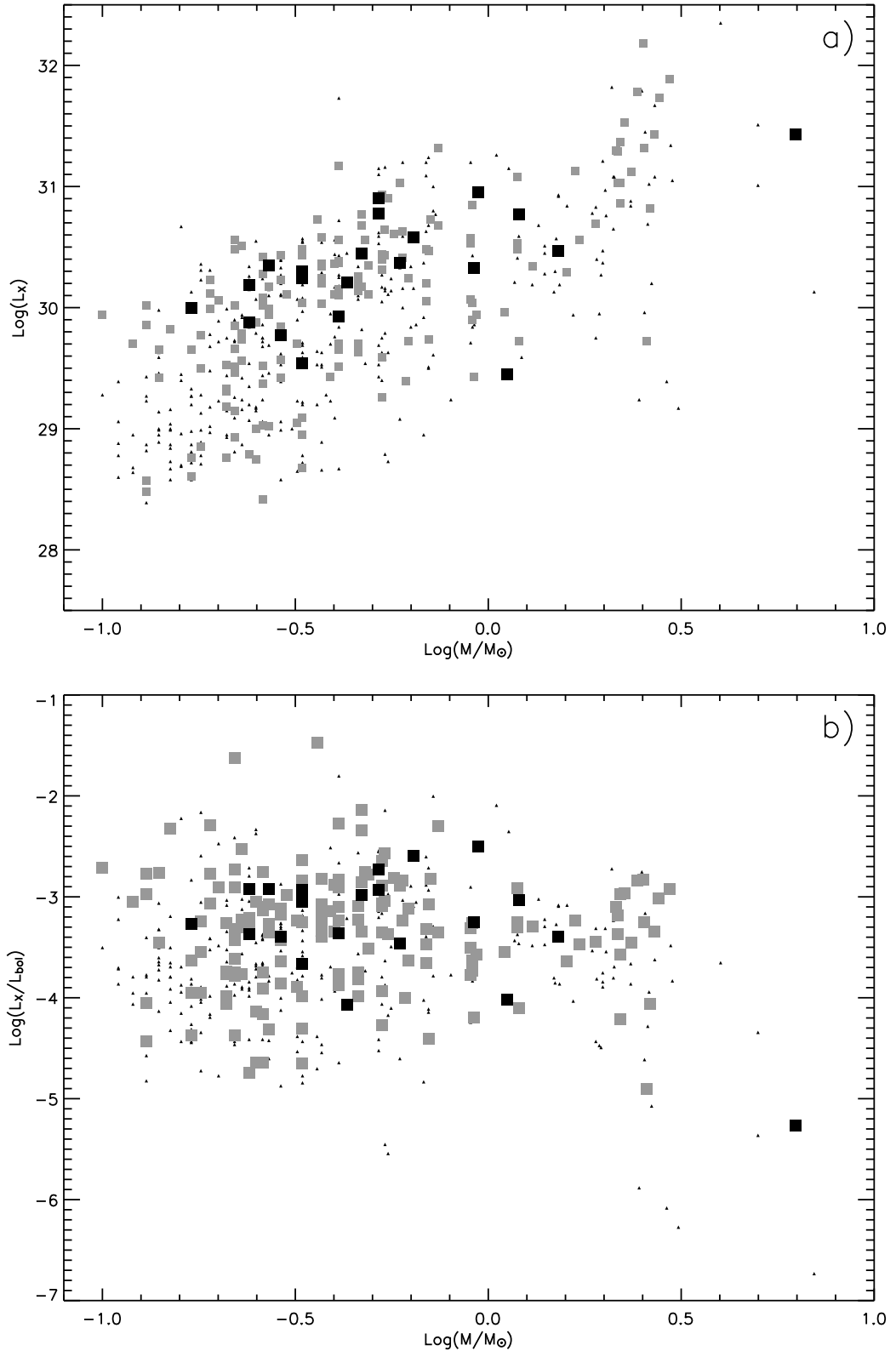


Fig. 9.— $\text{Log}(\text{Mass})$ vs. $\text{Log}(L_X)$ and $\text{Log}(L_X/L_{\text{bol}})$ for all COUP sources with mass estimates. Symbols as in Figure 8.

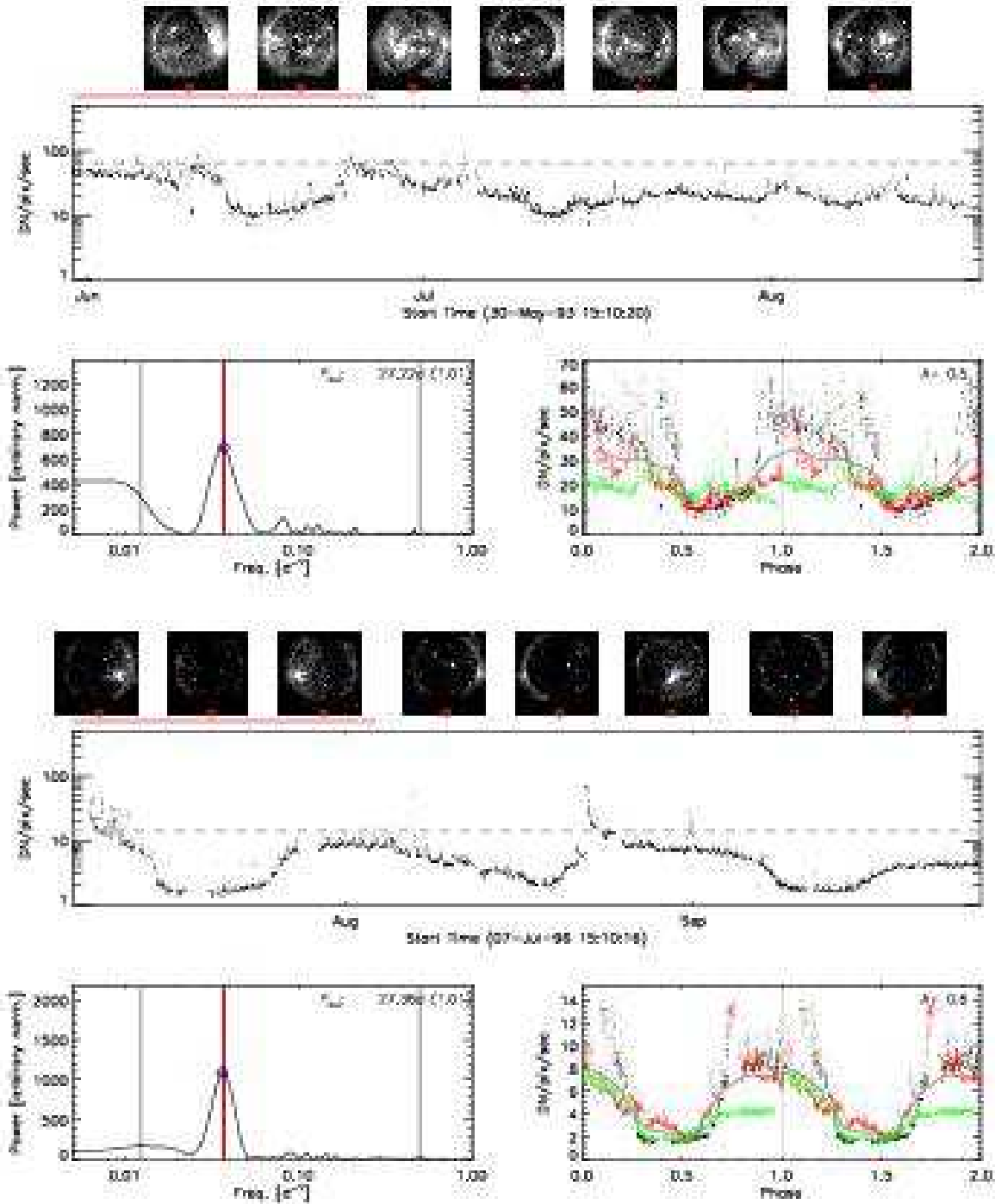


Fig. 10.— YOHKOH SXT (AlMg filter) light curves with relative full disk images (at selected times), periodograms and folded light curves, in a format similar to figure 2. The two sets of panels refer to different 81 days time segments: the upper one is close to solar maximum, the lower one to solar minimum.

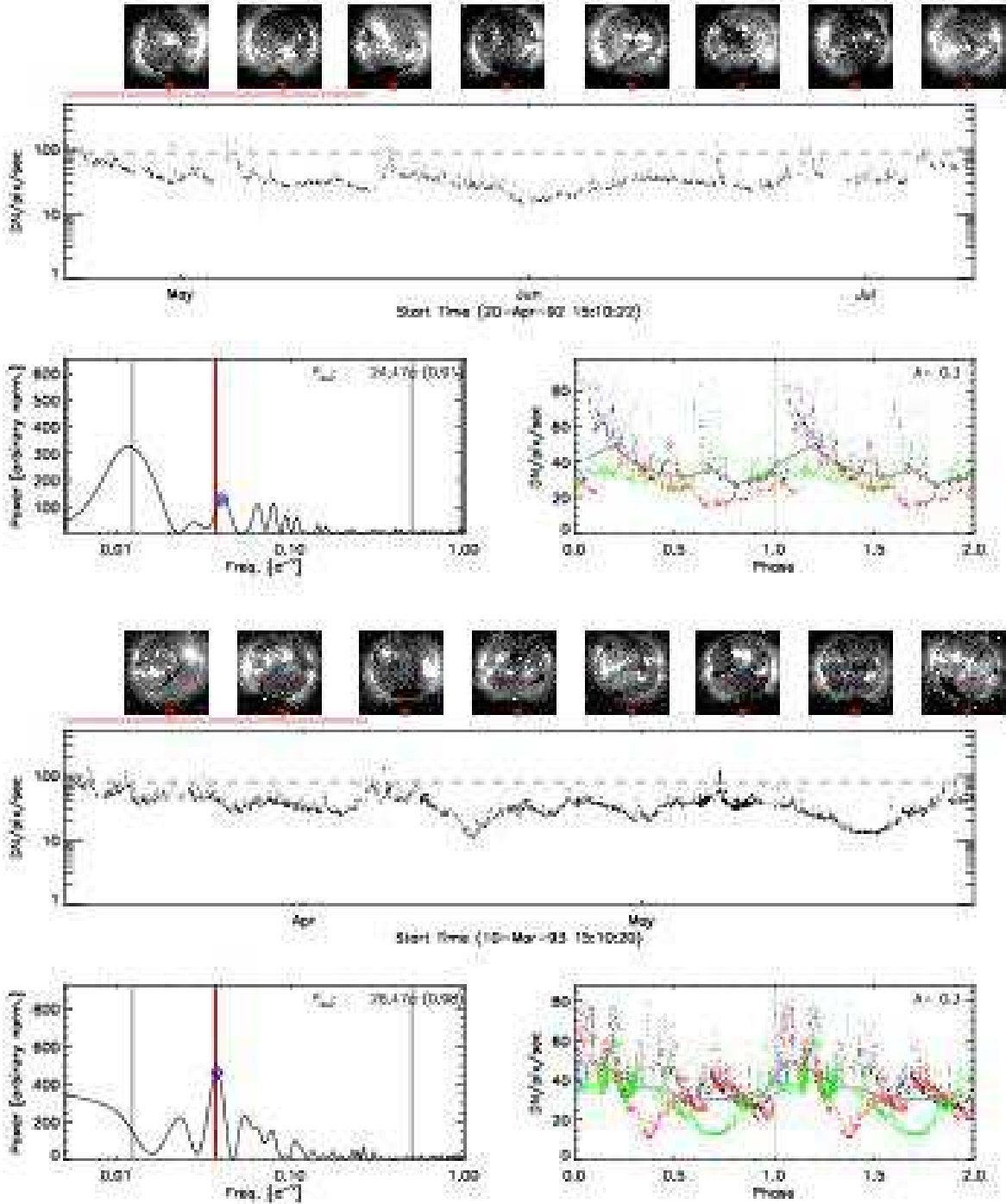


Fig. 11.— Same as figure 10, for two other time segments both close to solar maximum.

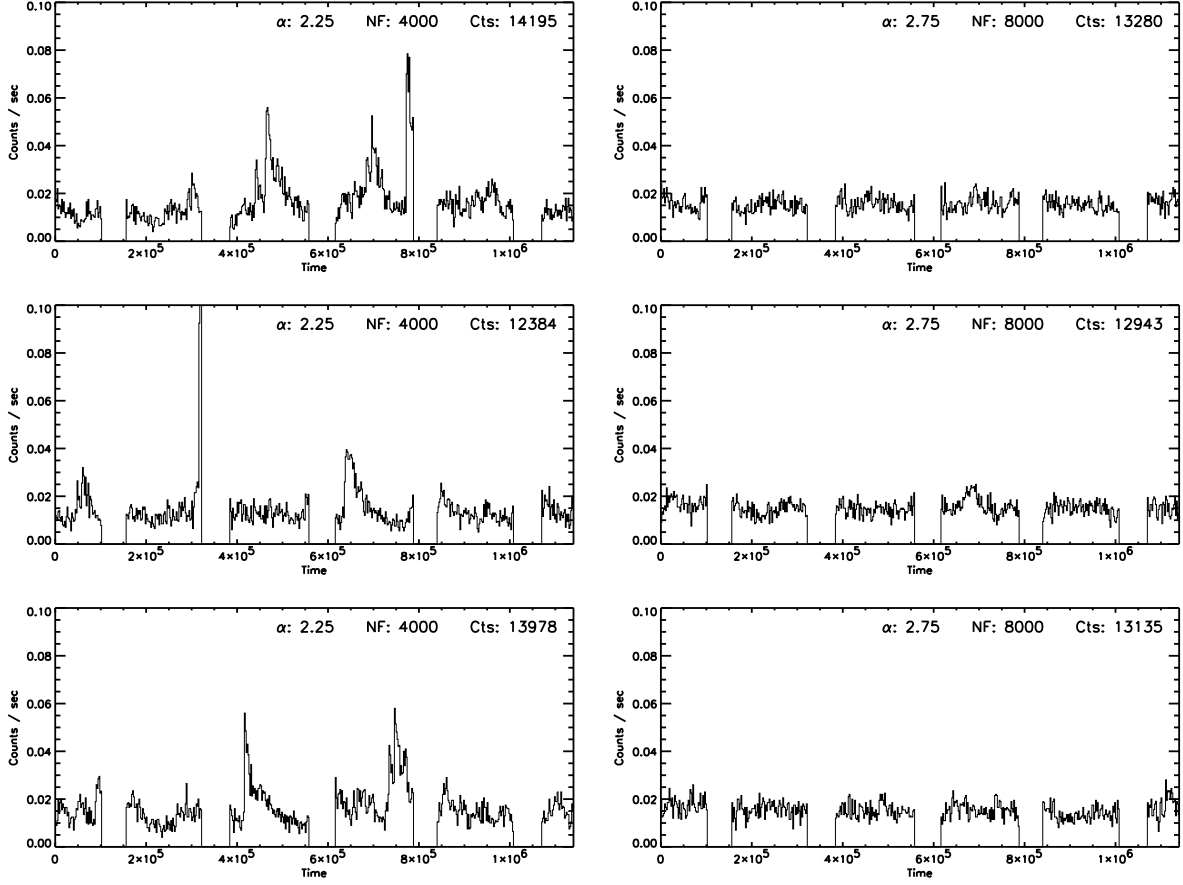


Fig. 12.— Example of six simulated lightcurves with no modulation, three for each of two values of the parameter α (= the slope of the flare intensity distribution): $\alpha = 2.25$ (left) and 2.75 (right). The number of simulated flares (NF), all having $\tau_{fl} = 5h$, is chosen so to yield, in the two cases, a similar average number of counts. The actual number of simulated counts is given in the upper right corner of each panel.

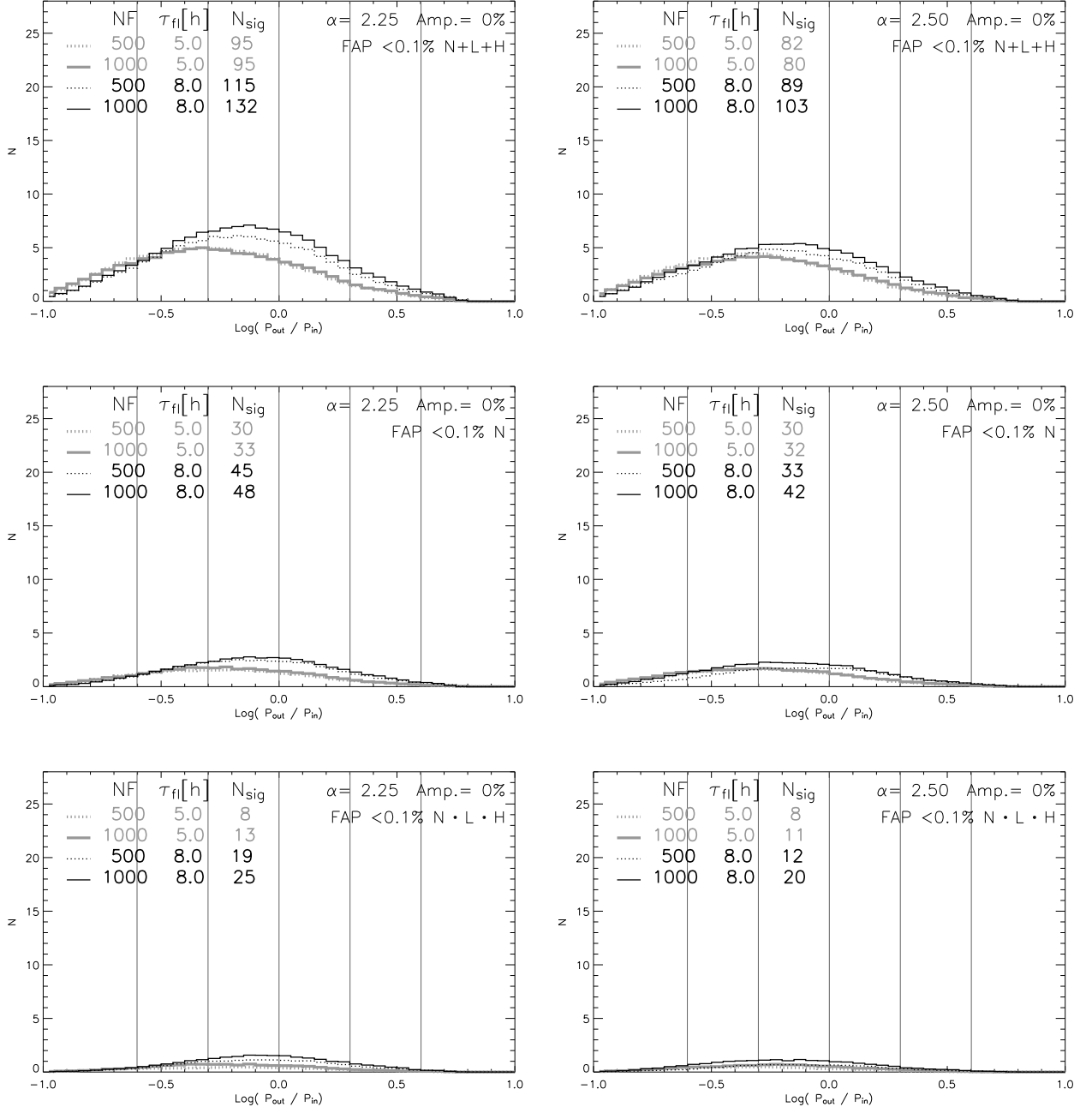


Fig. 13.— Histograms of $\log P_{out}/P_{in}$, resulting from the application of our period finding method to simulated “flaring” light curves (see text) with no intrinsic modulation (Amp=0%). Rows refer to three selections of “significant” periods, the same as in Figure 6. From top to bottom: “ $N+L+H$ ”, “ N ” and “ $N \cdot L \cdot H$ ”. The left and right columns refer to simulations with $\alpha = 2.25$ and $\alpha = 2.50$. Within each panel four histograms are shown, for NF=500 and 1000 and for $\tau_{fl} = 5$ and 8 hours, as indicated in the legend on the upper left of each panel. All histogram are normalized so to yield the expected distributions for a sample of 233 stars with P_{in} equal to P_{opt} in our “searched” sample. In the legend we also report the integral of these distributions, N_{sig} , indicating for each set of input parameters the total number of stars expected to pass the significance selections.

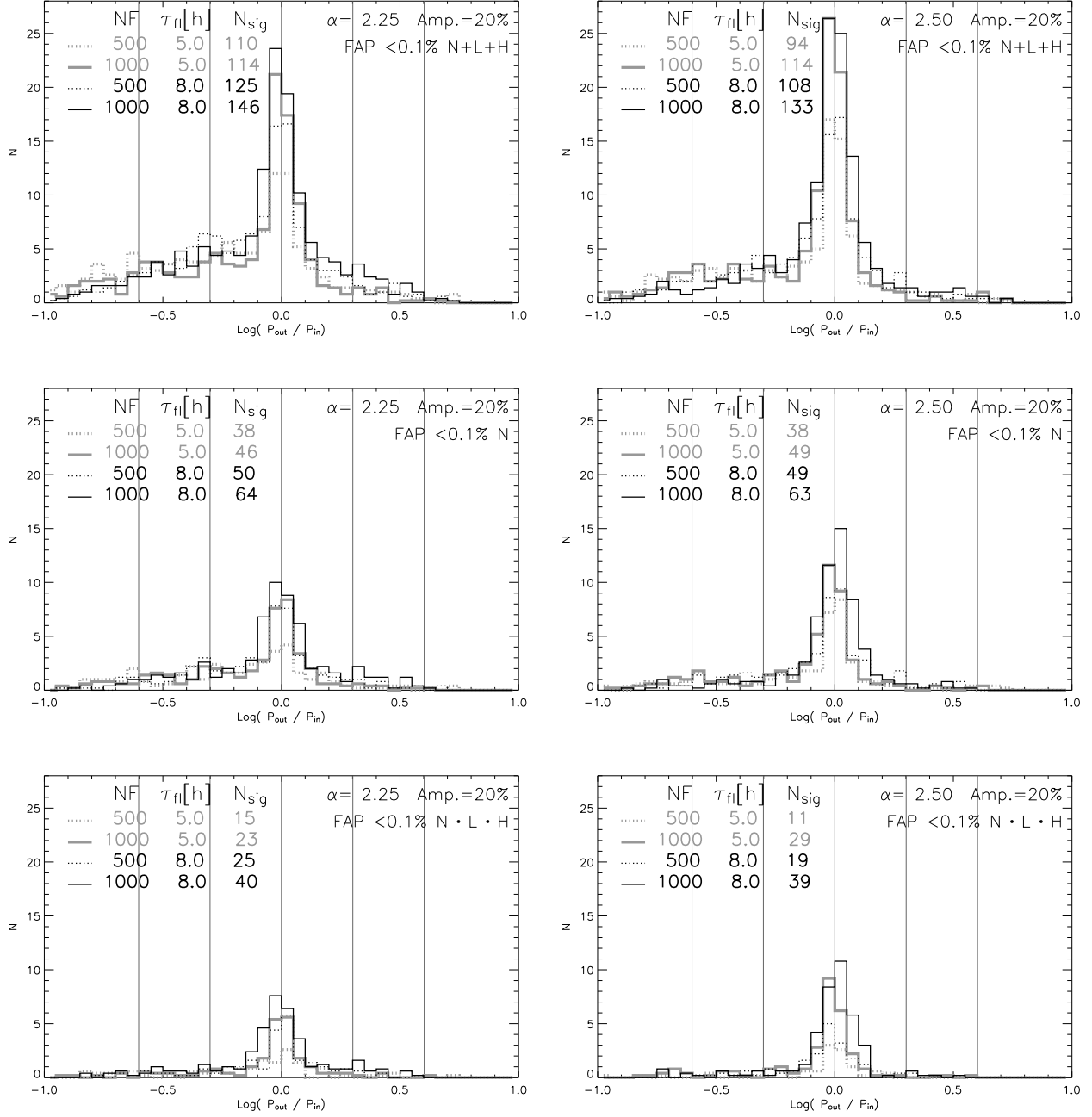


Fig. 14.— Same as Figure 13, but for simulated lightcurves with intrinsic 20% relative modulation.

This figure is available in the electronic version of ApJ. A version of the paper that includes the 34 panels of this figure can be downloaded from:

http://www.astropa.unipa.it/~ettoref/COUP_RotMod.pdf

Fig. 15.— Sources for which all filtering methods yield $\text{FAP} < 0.1\%$ (“ $N \cdot L \cdot H$ ” selection)